Epigenetic variation mediated by lncRNAs accounts for adaptive genomic differentiation of the endemic blue mussel *Mytilus chilensis*

Marco Yévenes [a,*], Cristian Gallardo-Escárate [b], Gonzalo Gajardo [a]

[a] *Laboratorio de Genética, Acuicultura y Biodiversidad, Departamento de Ciencias Biológicas y Biodiversidad, Universidad de Los Lagos, Osorno, Chile*
[b] *Centro Interdisciplinario para la Investigación en Acuicultura, Universidad de Concepción, Concepción, Chile*

A B S T R A C T

Epigenetic variation affects gene expression without altering the underlying DNA sequence of genes controlling ecologically relevant phenotypes through different mechanisms, one of which is long non-coding RNAs (lncRNAs). This study identified and evaluated the gene expression of lncRNAs in the gill and mantle tissues of *Mytilus chilensis* individuals from two ecologically different sites: Cochamó (41°S) and Yaldad (43°S), southern Chile, both impacted by climatic-related conditions and by mussel farming given their use as seedbeds. Sequences identified as lncRNAs exhibited tissue-specific differences, mapping to 3.54 % of the gill transcriptome and 1.96 % of the mantle transcriptome, representing an average of 2.76 % of the whole transcriptome. Using a high fold change value ($\geq|100|$), we identified 43 and 47 differentially expressed lncRNAs (DE-lncRNAs) in the gill and mantle tissue of individuals sampled from Cochamó and 21 and 17 in the gill and mantle tissue of individuals sampled from Yaldad. Location-specific DE-lncRNAs were also detected in Cochamó (65) and Yaldad (94) samples. Via analysis of the differential expression of neighboring protein-coding genes, we identified enriched GO terms related to metabolic, genetic, and environmental information processing and immune system functions, reflecting how the impact of local ecological conditions may influence the *M. chilensis* (epi)genome expression. These DE-lncRNAs represent complementary biomarkers to DNA sequence variation for maintaining adaptive differences and phenotypic plasticity to cope with natural and human-driven perturbations.

1. Introduction

The classical view of adaptation states that mutation-driven genetic variability is the fuel upon which natural selection shapes adaptive phenotypes. Changes in DNA nucleotide sequences affect the expression of coding and regulatory genes underlying these phenotypes and their dominant, additive, epistatic, or pleiotropic interactions [1]. However, genetic variation does not exclusively explain the full variation in ecologically relevant traits, as it also depends on a suit of epigenetic mechanisms such as DNA methylation, chromatin modifications, and non-coding RNAs [2–4]. Since environmental factors and developmental processes influence epigenetic

changes that can be inherited, they represent a complementary inheritance system to adaptation, providing a fast genomic organismic response to environmental perturbations [4–6].

Long non-coding RNAs (lncRNAs) are a class of non-coding RNAs longer than 200 nucleotides transcribed like mRNAs, with tissue-specific and spatiotemporal-related expression [7]; [8], lacking detectable conserved coding motifs or protein domains [9,10]. They are classified according to their proximity to protein-coding genes and their different processing mechanisms. In eukaryotic genomes, for example, there are promoter transcripts (PROMPTs), enhancer RNAs (eRNAs), long intervening/intergenic ncRNAs (lincRNAs), and antisense transcripts (NATs) [11,12]. Additionally, lncRNAs may be found in intergenic and intronic regions and transcribed in a sense, antisense, or bidirectional orientations relative to their neighboring protein-coding genes [13]. LncRNAs can regulate gene expression through chromatin remodeling, promoter activation, activation and recruitment of transcription factors, or transcription interference [10,14,15]. These processes may involve both neighbor (*cis*-regulation) and distant genes (*trans*-regulation) with different regulatory effects [12,16,17]. For example, in marine pearl oysters, *Pinctada fucata*, the expression of *lncIRF-2*, located in an intron of the *Interferon regulatory factor 2* gene (PfIRF-2), has a positive regulatory effect on *Interleukin-17* gene (PfIL-17) but a negative regulatory effect on their neighbor protein-coding PfIRF-2 gene [18].

It is challenging to establish functions for specific lncRNAs, given the complex epigenetic regulatory networks, gene interactions, and additive effects on their related *cis* and *trans* gene regulation [14,19]. However, the expression patterns of some lncRNAs can be modulated by different stimuli, both in terrestrial organisms [20,21] and marine vertebrates [22–24] and invertebrates [8]; [25–27]. For example, marine mollusks experiencing different experimental conditions exhibited differentially expressed lncRNAs related to shell formation [28], pigmentation [29], larval development [30] and immune response [26]. In the gills of *Mytilus galloprovincialis* individuals, lncRNAs and their neighboring protein-coding genes (hereafter NPC-genes) showed differential expression after being challenged against *Vibrio splendidus* [31]. Mussels of the same species [27], exposed to three different pathogen-associated molecular patterns (PAMPs), differentially expressed protein-coding genes related to immune response, which appeared flanked by also differentially expressed lncRNAs by PAMPs, suggesting a *cis*-lncRNA effect. Together, these results reflect that lncRNAs play a relevant role in evolutionary change and ecological adaptation by regulating gene expression in response to environmental changes. Despite not encoding proteins, they interact with cellular molecules, modulating key genes in adaptive pathways. This influence extends to diverse biological processes, enhancing adaptive-related phenotypes in mussels (immunity, shell formation, larval development, and stress). As a result, these epigenetic factors are essential for understanding how organisms thrive in diverse habitats.

Consequently, this study investigates epigenetic variation mediated by lncRNAs in the endemic mussel *Mytilus chilensis*, a species heavily exploited in southern Chile due to its aquaculture importance [32,33]. This ecosystem engineer [32,33] is a close relative of the northern hemisphere *M. edulis* species complex [34,35]. It inhabits rocky substrates of intertidal and subtidal zones along the coasts of the South Pacific Ocean, from Bío-Bío (38°S) to Magallanes (53°S) [36], and has been used to explore issues in ecology [37], ecophysiology [38], and adaptive genomics [39,40]. This gonochoric species has an annual gametogenic cycle, reaching sexual maturity in spring-summer. After fertilization, their planktonic larvae can drift in the water column between 20 and 45 days before settling [41,42], being able to reach up to 30 km [43], facilitating different gene flow levels between locations [35,44,45]. For example, the genetic divergence between individuals from different locations, estimated by the use of genetic (*COI* gene, microsatellites) and genomic (SNPs outliers) population markers, has been described as low but significant ($F_{ST}\sim0.04$, $p_{value}< 0.05$) [44–47]. Thus, a single reproductive unit would exist in southern Chile without any discrete regional stocks, except for Punta Arenas in Magallanes [48].

Economically, this species sustains a world-class farming industry [49] concentrated in the inner sea of Chiloé Island (41°S to 44°S), an industry entirely depending on the availability of juvenile individuals (seeds) artificially collected from natural seedbeds, which are transferred to ecologically heterogeneous bays until harvest. Due to the continued extraction of genotypes and lack of natural recruitment, some of these natural seedbeds have reduced size and exhibit high inbreeding values [46]. Cochamó and Yaldad are two natural seedbeds located in the northern and southern zones of the inner sea of Chiloé Island, respectively [44,47]. Both locations are separated by about 250 km and by a north-south gradient of seawater temperature, currents, salinity, and chlorophyll-a concentration [50–52]. In this context, besides the extraction of selected commercial phenotypes, the production cycle considers seed translocations from seedbeds, facilitating hybridization between individuals from relatively divergent locations, increasing the risk of a loss of locally adapted alleles and the erosion of genetic diversity [53]. However, translocated individuals also are exposed to a wide range of potentially pathogenic microorganisms [54,55], contamination [56,57], and environmental variability [58–60]. These factors can affect mussel health, shell biomineralization, reproductive performance, larval recruitment, and population growth [61–64]. In short, their fitness response is high in their local environment [65]. Examples are the adaptive differences in gene expression and monomorphic genetic variants in whole and mitochondrial transcriptomes of gill and mantle tissues of native individuals from Cochamó and Yaldad, published by Yévenes et al. [39,40]. These differences involve metabolic processes, immune response, and genetic information processing (replication, transcription, and translation) related to differences in temperature and salinity of seawater, presence of xenobiotics, and shell biomineralization.

Given the importance of epigenetic diversity for evolutionary change and adaptation to heterogeneous environments [4–6], this investigation proposes that differentially expressed lncRNAs present in the *M. chilensis* genome contribute to the adaptive differences in gene expression detected in individuals from these two ecologically contrasting seedbeds. This proposition is now amenable to testing with the annotated whole genome sequence of *M. chilensis* already published [66]; hence, it is possible to identify genomic lncRNAs in these individuals and assess their differential expressions and the NPC-genes they could be modulating. This study aims to identify genomic lncRNAs and investigate how their tissue and geographic location-driven differential expressions could relate to the differential expression of adaptive candidate NPC-genes revealed by the species transcriptome analysis [39]. This knowledge should provide insights into how, collectively, epigenetic and genetic differences in natural farm-impacted seedbeds, such as Cochamó and

Yaldad, may contribute to the persistence of populations of this species.

## 2. Materials and methods

2.1. Study sites and sampling

Raw oceanographic data on temperature (°C), currents (m/s), salinity (psu), and age of seawater (days) as an estimate of dissolved oxygen [67] were collected from the CHONOS database (http://chonos.ifop.cl/), managed by the Instituto de Fomento Pesquero, IFOP (Institute of Fisheries Enhancement), for Cochamó (41° 28′ 23″ S – 72° 18′ 38″ W) and Yaldad (43° 70′ 14″ S – 73° 44′ 25″ W). The data (0 to −10 m deep) are for June 2017 to May 2018, which overlaps with this study's sampling date (Fig. 1). Data were projected and visualized with Ocean Data View ODV v5.32 software (https://odv.awi.de/).

2.2. lncRNA mining and database construction

This study used 12 cDNA libraries sequenced through RNA-Seq, previously published [39] and available in GenBank as BioProject accession number PRJNA630273. These libraries were also utilized for the differential expression analyses in complete transcriptomes. They represent the total RNA extracted from gill and mantle tissues from 15 individuals randomly collected in Cochamó and Yaldad on April 26, 2018. The 15 total RNA extractions per tissue were grouped into three sets of samples, each composed of 5 individual extractions with equimolar quantities of total RNA. Thus, three libraries represent each location's biological replicates of gill and mantle tissue.

The clean reads and the transcriptome reference library (TRL) documented in Yévenes et al. [39] were also harnessed in this study. Briefly, the assembly of this TLR encompassed trimming raw data for each library and conducting de novo assembly using CLC Genomic Workbench software v21.0.3 (Qiagen Bioinformatics™). The filters were conducted to obtain clean reads, using a quality score of 0.05, removal of low-quality sequences, mismatch cost of 2 and 3 for insertions and deletions, length of 0.8, and similarity fractions of 0.9 with a maximum of 10 hits per read. The TRL was constructed de novo utilizing all samples, resulting in 189,743 consensus contigs, each with a minimum length of 200 base pairs. This TRL was employed for lncRNA mining and constructing the lncRNA database.

The TRL was instrumental in selecting putative lncRNAs through an adapted pipeline as previously outlined [27]. The contigs within the TRL underwent annotation via BLASTx against the UniProt/SwissProt database (with an $e_{value} < 1E-5$), accessible within the NCBI nucleotide repository. Homology searches considered the NCBI EST database using the tBLASTx algorithm to detect potential
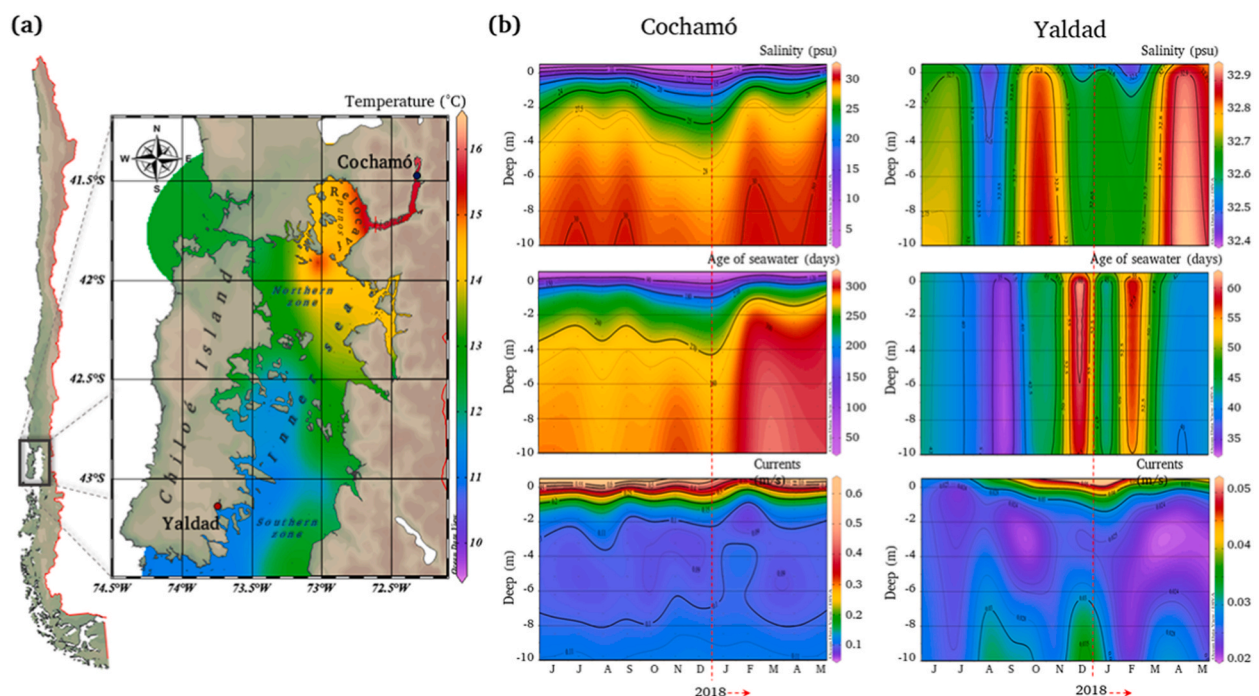
Fig. 1. Map of sampling locations.
Map (**a**) with the geographic location of the sampled natural seedbeds of *Mytilus chilensis*, Cochamó (north), and Yaldad (south) of Chiloé Island. Mean seawater temperature (colored background) between June 2017 and May 2018. (**b**) Mean seawater of salinity, age of seawater, and currents for each sampling location. The scaling of the parameters is different between locations.

transcripts. Contigs with annotations from the TRL and transcripts displaying open reading frames (ORFs) exceeding 200 base pairs were excluded. Subsequently, sequences displaying coding potential were discarded using the Coding Potential Assessment Tool (CPAT) [68]. Only contigs from the TRL that successfully passed all the filtering steps were considered for the final *M. chilensis* lncRNA database used in the following analyses.

2.3. RNA-Seq and differential expression analysis

Using 43,011 non-coding sequences from the *M. chilensis* lncRNA database as a reference, we conducted two RNA-Seq analyses to identify distinct lncRNA expression patterns in *M. chilensis* transcriptomes. Firstly, the analysis compared lncRNA expression between tissues (gills and mantles) by independently mapping clean reads. Subsequently, the evaluation extended to analysing lncRNA expression between locations, disregarding tissue origin, by collectively mapping clean reads from gill and mantle samples at each location.

The CLC Genomic Workbench (CLCgw) software was also employed to map, normalize, and quantify the clean reads from the samples using the tools available within the RNA-Seq analysis suite. The software allowed estimating transcripts per million (TPM) values as a proxy of lncRNA expression levels by aligning reads with the *M. chilensis* lncRNA database globally. We applied filters to align one gene per transcript during read mapping to ensure robustness and reduce biases. These filters included a mismatch cost of 2, a maximum cost value of 3 for insertions and deletions, length and similarity fractions of 0.8, and a maximum limit of 10 hits per read. Transcripts from all samples that contained invalid values or had zero read counts were excluded from the analysis. A negative binomial generalized linear model (GLM) was employed for differential expression analyses to assess the significance of variations. This model aimed to determine if differences attributed to sample origin (tissue and location) deviated from zero. The Wald test was used to test for statistical assessment. Fold change values were estimated from the GLM model to correct for the differences in library size between samples and the effects of biological replicates.

Within the biological context of this research, which involves native individuals from two ecologically contrasting locations, two different filters were used to explore the differential expression of lncRNAs. Initially, more lenient fold change values (FC_{value}) thresholds were utilized to explore sample variability and identify noteworthy gene expression differences, mitigating the risk of Type I error. These thresholds encompassed an FC_{value} of $\geq|4|$ and an adjusted p_{value} for controlling the false discovery rate (FDR) at ≤ 0.05. The outcomes of analyzing the 12 sequenced cDNA RNA-Seq libraries were portrayed through cluster heatmaps, organized on tissue and location using Euclidean distances and average linkage. Additionally, the differential expression of lncRNAs was statistically assessed using principal component analysis, and the relationship between $-\log_{10}(p_{values})$ and $\log_2$(fold change) values was graphically examined using volcano plots. Subsequently, a more stringent fold change threshold and adjusted p_{value} were implemented to diminish the potential for false positives stemming from multiple comparisons. These thresholds encompassed an $FC_{value} \geq|100|$ and Bonferroni-corrected $p_{value} \leq 0.05$ for tissue comparisons and FDR $p_{value} \leq 0.05$ for comparison between locations, which focused on identifying lncRNAs with high and significant fold change values. Venn diagrams facilitated sample comparison, enabling the identification and selection of DE-lncRNAs meeting these criteria. Opting for this filter aimed to highlight those lncRNAs with evident and possibly striking differences in the biological context explored, despite the inherent risk of filtering out lncRNAs with low fold change but with putative relevant biological effects. Accurately identifying these lncRNAs presents challenges, given their expression similarities with less biologically influential counterparts. Alternative analytical approaches (p.ej., cloning) could be a valuable strategy to address this issue. In this study, the lncRNAs that passed stringent filters on each comparison were identified and selected as significantly differentially expressed lncRNAs (DE-lncRNAs), and their sequences were extracted and annotated.

2.4. DE-lncRNAs and neighboring genes positioning and extraction

The genomic position of DE-lncRNAs was determined by mapping them against the whole genome sequence of *M. chilensis*, whose assembly is described in detail in Ref. [66]. These mapping processes were facilitated also using the CLCgw software. The output files from the mappings were exported in SAM format and uploaded to GALAXY [69] online server (https://usegalaxy.org/) and converted into interval, BED, and GFF formats for upload to the CLCgw for further annotation of lncRNAs in the genome. The extract annotations tool available in CLCgw identified those NPC-genes flanking up to 10 kb up and downstream from the DE-lncRNA of the samples.

2.5. DE-lncRNAs annotations on available web databases

The annotations and functional categorizations of the identified DE-lncRNAs in *M. chilensis* were screened using the available lncRNAs databases on the web. LncLocator [70] facilitated predictions regarding the subcellular localization of DE-lncRNAs (http://www.csbio.sjtu.edu.cn/bioinf/lncLocator/). RNAcentral (https://rnacentral.org/) was employed to perform sequence comparisons, offering information about the number of hits aligning with the DE-lncRNA sequences. This information included valuable data such as e_{values} and identity percentages concerning homologous lncRNAs from the closely related species *M. galloprovincialis*.

The outputs from the RNAcentral database were instrumental in gleaning information about homologous sequences, thereby aiding in identifying DE-lncRNAs detected in *M. chilensis*. This database encompassed details such as names, aliases, and connections to other databases, including, for example, LncBook (https://ngdc.cncb.ac.cn/lncbook/home/), NONCODE (http://www.noncode.org/index.php/), e!Ensembl (https://www.ensembl.org/index.html/), GeneCards (https://www.genecards.org/), and LNCipedia (https://lncipedia.org/). These resources provided insights into the classification of lncRNAs and their ontological characterization based on analogous lncRNAs identified in other species.

2.6. GO analysis of neighboring protein-coding genes

For the selected DE-lncRNAs in each comparison by tissue and location, their corresponding extracted NPC-genes (10 kb up- and downstream) were GO enriched. The NPC-gene sequences underwent enrichment analysis using a hypergeometric distribution model executed on the KOBAS [71] online server (http://bioinfo.org/kobas/genelist/). This analysis considered the mollusk database of *Crassostrea gigas* as a reference. The outcomes of this analysis yielded a list of GO ID terms. Subsequently, the REVIGO [72] online server (http://revigo.irb.hr/) was employed to refine the results. Fisher's exact test was conducted (with default settings) to assess the over-representation of GO terms, aiming to distill the most specific GO ID terms. Semantic graphs visually presented the results, depicting the most enriched GO ID terms across biological processes, cellular components, and molecular functions. This analysis allowed insights into the functional implications of the DE-lncRNAs and their linearly linked NPC-genes in the samples from both locations.

2.7. DE-lncRNA and differential expression comparison of NPC-genes

The previously published transcriptomic analyses [39] for these same individuals from Cochamó and Yaldad were used to assess the differential expression of the NPC-genes linearly linked to the DE-lncRNAs, detected in both comparisons by tissue and location. Specifically, this study used Supplementary Tables 3 and 6 to identify differentially expressed transcripts (DETs) in complete transcriptomes. The DETs were extracted from these tables along with their FC_{value} and mapped over the NPC-gene sequences. The filters used for the mappings included a match score of 2, mismatch cost of 4, gap open cost of 4, gap extend cost of 2, long gap open cost of 24, and long gap extend cost of 1. Those DETs aligned with the selected NPC-genes sequences were identified and extracted. The FC_{value} of these extracted DETs was considered the expression value of their corresponding NPC-mapped gene. This FC_{value} was contrasted with the FC_{value} of its corresponding DE-lncRNA.

3. Results

3.1. Environmental characterization

The analysis of the environmental raw data (**Supplement 1**) collected from CHONOS database allowed identified oceanographic differences (0 to −10 m) between the seedbeds from June 2017 to May 2018 (Fig. 1). Cochamó exhibited higher temperatures, sea currents, and longer water retention time than Yaldad but lower salinity, supporting the idea that they correspond to ecologically different zones in the inner sea of Chiloé Island, north and south.

3.2. Tissue and location mapping of reads

The mapping of the clean reads showed that the gill samples of individuals from both locations had a higher percentage of mapped reads than the mantle samples (Table 1). Mapping by biological replicates (Table 1a) shows an average of 3.47 % of the 40.25 million reads from Cochamó gill samples (LCo_g) mapped against the *M. chilensis* lncRNA database. Similarly, 3.61 % of the 39.2 million reads from Yaldad gill samples (LYa_g) were mapped against the database. Likewise, 2.05 % of the reads from Cochamó mantle samples (LCo_m) and 1.87 % from Yaldad (LYa_m) were mapped. Such tissue differences in the percentage of mapped reads were confirmed when clean reads from replicates were mapped together (Table 1b). LCo_g samples showed more mapped reads (3.49 %) than their LCo_m counterparts (2.05 %). The Yaldad gills (LYa_g) and mantle (LYa_m) showed 3.62 % and 1.87 % of reads mapped, respectively.

Table 1

Characteristics of the mapping outlined for replicates (**a**) and tissues (**b**), using clean reads from Cochamó and Yaldad samples. These clean reads were aligned against the reference sequences contained in the *M. chilensis* lncRNA database. Labels: LCo_g/m (Cochamó gills/mantle), LYa_g/m (Yaldad gills/mantle).

a. Mapping by replicate							
Cochamó	Replicate	**LCo_g1**	**LCo_g2**	**LCo_g3**	**LCo_m1**	**LCo_m2**	**LCo_m3**
	Number of reads	31,763,950	51,520,578	37,459,046	42,308,892	35,879,760	39,073,458
	Reads mapped in pairs	1,040,406	1,819,676	1,352,786	843,538	759,694	798,388
	% Reads mapped in pairs	3.28	3.53	3.61	1.99	2.12	2.04
Yaldad	Replicate	**LYa_g1**	**LYa_g2**	**LYa_g3**	**LYa_m1**	**LYa_m2**	**LYa_m3**
	Number of reads	33,296,098	38,652,662	36,636,826	36,485,868	41,935,332	37,139,370
	Reads mapped in pairs	1,184,844	1,450,336	1,292,728	682,734	790,014	686,172
	% Reads mapped in pairs	3.56	3.75	3.53	1.87	1.88	1.85

| b, Mapping by tissue				
Tissue	**LCo_g**	**LCo_m**	**LYa_g**	**LYa_m**
Reads mapped in pairs	4,212,868	2,401,620	3,927,908	2,158,920
% Reads mapped in pairs	3.49	2.05	3.62	1.87

3.3. Tissue-specific differential expression of lncRNAs

Regarding tissue comparison, the lenient filters ($FC_{value} \geq |4|$ and FDR $p_{value} \leq 0.05$) revealed significant differential expression profiles between samples. Euclidean distances between the expression values showed the lncRNAs contigs grouped into two larges differentially expressed lncRNAs (DE-lncRNAs) clusters in the heatmap (Fig. 2a): the up-regulated ones in the Cochamó and the Yaldad samples. Also, the LCo_g and LCo_m samples were similar to each other than LYa_g and LYa_m profiles. Principal component analysis (PCA), as depicted in Fig. 2b (**Supplement 2**), validates the observed expression differences. The analyses discern that 55.8 % of the variability stems from sample origin (Cochamó or Yaldad), and 24 % is associated with tissue variation (gill or mantle). These distinctions gain additional support from the symmetrical data distribution in the $-\log_{10}(p_{value})$ vs. $\log_2$(fold change), featured in the volcano plot of Fig. 2c. The number of tissue-specific differentially expressed lncRNAs (DE-lncRNAs) within each group was 621 DE-lncRNAs in Cochamó and 383 in the Yaldad samples. From these, 347 were exclusive of Cochamó and 109 of Yaldad (Fig. 2d). With the stringent filters used ($FC_{value} \geq |100|$ and Bonferroni $p_{value} \leq 0.05$), Cochamó individuals exhibited a higher number of DE-lncRNAs in gills (43) and mantle (47) than Yaldad, 21 and 17 in gills and mantle, respectively. These last significant DE-lncRNAs were identified and selected for further annotations.

3.4. Location-specific differential expression of lncRNAs

The comparison between the expression values by location using the lenient filters showed differential expression of 215 putative lncRNAs from the Cochamó (LCo) and 172 from Yaldad samples (LYa). The stringent filters also resulted in different numbers of significant DE-lncRNAs between Cochamó (65) and Yaldad (94) (**Supplement 3**). These significant DE-lncRNAs also were identified and selected for further annotations.

3.5. Annotation of DE-lncRNA using available databases

Different web databases provided information on homologous sequences of the DE-lncRNAs detected in *Mytilus chilensis* transcriptomes. About 78 % of these sequences were predicted to be of nuclear localization, while 22 % were cytoplasmic. Likewise, about 55 % were assigned as lincRNAs (long intervening/intergenic ncRNAs), 28 % as antisense, and 15 % as intronic. The list in Table 2 shows collected information for the top ten DE-lncRNAs with the highest FC_{value} for tissue comparisons, among them, the predicted subcellular location, the class of each DE-lncRNA, and the name of the closest lncRNA homolog. The table also shows the number of hits from the search for lncRNAs in the RNACentral database and the number of homologous sequences found in the sister species *M. galloprovincialis*. About 78 % of the identified *M. chilensis*'s DE-lncRNAs corresponded to more than ten similar sequences in *M. galloprovincialis*, with an average e_{value} of 1e+04, and an average identity of 62 %. However, in most cases, the percentage of
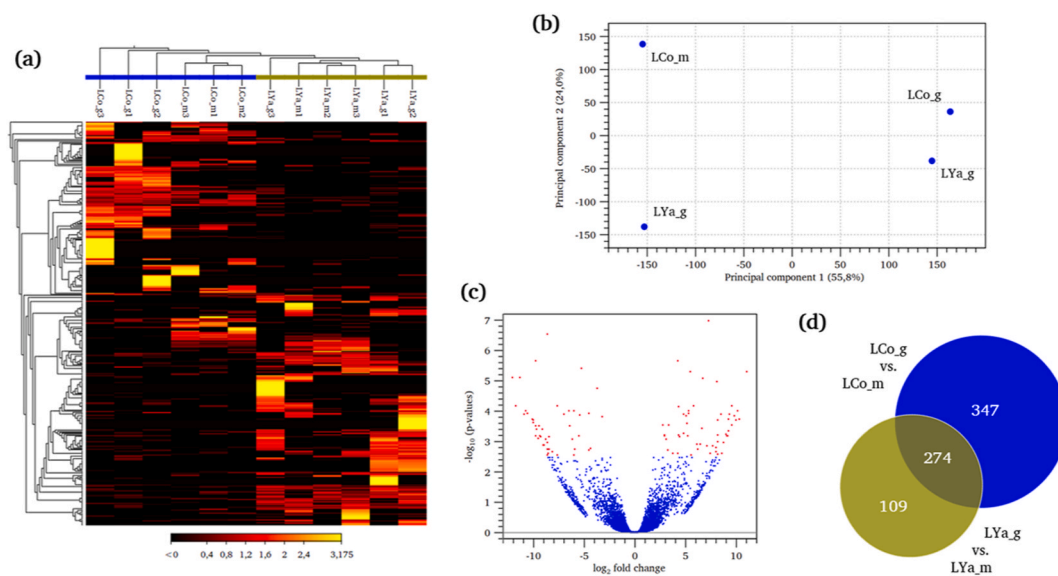
Fig. 2. Differential expression of lncRNAs in *Mytilus chilensis*.
Heatmap (a) illustrating expression variations patterns among samples grouped by tissue and location, constructed using cut-offs of fold change (FCvalue) > |4| and FDR p_{value} <0.05. Exploring the magnitude of expression differences in lncRNAs from analyzed samples are highlighted in the PCA and volcano plots (b and c, respectively). Red points in (c) denote Bonferroni p_{value} filtered outcomes. These last were selected and enumerated using (d) Venn diagram, where the numbers represent the count (exclusive and shared) of differentially expressed lncRNAs (FCvalue>4; Bonferroni p_{value}<0.05) for each comparison. Labels: LCo_g/m (Cochamó gills/mantle), LYa_g/m (Yaldad gills/mantle). (For interpretation of the references to color in this figure legend, the reader is referred to the Web version of this article.)

Table 2

Annotations for the top ten tissue-specific, differentially expressed lncRNAs identified through online database analysis. Labels: FC_{value} (Fold change value), MG (*Mytilus galloprovincialis*), LCo_g/m (Cochamó gills/mantle), LYa_g/m (Yaldad gills/mantle).

Samples	Query lncRNA Contig	FC_{value}	lncLoc Location	LNCPedia Sequence Ontology class	LNCPedia & LncBook Gene Name	RNACentral Hits	RNACentral MG Hits	RNACentral MG ID	e-value	Identity (%)
LCo_g	Contig_0009434_	3416	Nucleus	lincRNA/intergenic/antisense	lnc-NXPH1-2	482	9	URS00021A9E09_29158	4.5e+03	66.7
	Contig_0053071_	2495	Nucleus	Antisense	HSALNG0067894	694	18	URS000218D0FD_29158	1.1e+01	56.0
	Contig_0118039_	2481	Cytoplasm	lincRNA/intergenic/antisense	Lnc-FRG2C-5	184	6	URS000219B59F_29158	1.0e-124	98.2
	Contig_0166152	2257	Nucleus	Antisense	HSALNG0130830	288	2	URS00021C0FC5_29158	1.3e-02	58.8
	Contig_0087233_	1982	Nucleus	lincRNA/intergenic/antisense	lnc-ASB9-2	185	2	URS00021D0278_29158	4.6e+03	47.4
	Contig_0043161_	1941	Nucleus	lincRNA/intergenic/antisense	Lnc-ATG5-31	346	2	URS00021E4514_29158	2.8e+04	60.5
	Contig_0099084_	1705	Nucleus	Intronic/sense	Lnc-GSX2-1	438	12	URS000219561A_29158	1.4e+03	66.7
	Contig_0108244_	1662	Nucleus	Antisense	CALML3-AS1	259	2	URS00021AB5FE_29158	4.7e+04	64.1
	Contig_0184225	1265	Nucleus	lincRNA/intergenic	HSALNG0049232	25	1	URS00021A2D91_29158	2.1e+04	55.1
	Contig_0176068	776	Cytoplasm	Intronic/sense	lnc-PLA2G4F-3	62	–	–	–	–
LCo_m	Contig_0171681	−1400	Nucleus	Antisense	HSALNG0072944	171	4	URS00021D6B21_29158	8.4e+03	68.1
	Contig_0188421	−968	Nucleus	lincRNA/intergenic	HSALNG0045657	815	757	URS00021E994E_29158	1.2e-08	54.6
	Contig_0054268_	−536	Cytoplasm	Antisense	lnc-CREB5-2	766	9	URS00021AABEF_29158	2.2e+03	58.0
	Contig_0059020_	−516	Nucleus	Intronic/sense	lnc-TNFRSF19-8	256	6	URS00021EB48D_29158	4.8e+04	61.4
	Contig_0158861	−516	Nucleus	lincRNA/intergenic	lncRNA 1312	78	5	URS00021B734A_29158	4.9e+3	63.5
	Contig_0090188_	−509	Cytoplasm	lincRNA/intergenic	lnc-SH2D1B-5	382	16	URS00021DF148_29158	5.5e+03	65.4
	Contig_0184493	−379	Nucleus	lincRNA/intergenic	lnc-BCAS1-6	36	–	–	–	–
	Contig_0068815_	−348	Nucleus	Antisense	lnc-COL28A1-1	213	14	URS00021BAFFC_29158	4.8e+03	58.8
	Contig_0139582	−344	Cytoplasm	lincRNA/intergenic	HSALNG0026539	199	1	URS00021B3785_29158	6.4e+04	65.5
	Contig_0159625	−341	Nucleus	Intronic/sense	lnc-EHHADH-1	162	5	URS00021D69B0_29158	1.7e+00	58.9
LYa_g	Contig_0103992_	12,514	Nucleus	lincRNA/intergenic	HSALNG0101238	176	5	URS00021A23F3_29158	4.1e+03	66.2
	Contig_0043791_	5981	Nucleus	Antisense/bidirectional promoter	lnc-PRSS27-2 -4	217	6	URS00021B053A_29158	7.4e+02	55.5
	Contig_0053558_	2435	Cytoplasm	lincRNA/intergenic	lnc-OR5AK2-1	635	40	URS0002195345_29158	6.0e+03	64.3
	Contig_0069641_	741	Nucleus	lincRNA/intergenic	HSALNG0109213	248	8	URS00021D8DA0_29158	5.3e+02	56.1
	Contig_0167221	486	Nucleus	Antisense	HSALNG0053093	37	–	–	–	–
	Contig_0150090	405	Nucleus	Intronic/sense	lnc-ABCA9-5	79	–	–	–	–
	Contig_0141412	356	Nucleus	Antisense	lnc-BNIP2-4	50	1	URS00021BAFF4_29158	6.4e+04	62.5
	Contig_0013111_	306	Nucleus	lincRNA/intergenic	Lnc-PTER-2	407	9	URS00021B0BBA_29158	6.2e-01	54.0
	Contig_0003822_	299	Nucleus	lincRNA/intergenic	Lnc-FOXL1-2	727	54	URS00021C466_29158	6.2e+00	58.1
	Contig_0132878	296	Cytoplasm	lincRNA/intergenic	Lnc-HNRNPA2B1-4	117	3	URS00021E4116_29158	1.7e-10	59.5
LYa_m	Contig_0118050_	−2714	Cytoplasm	lincRNA/intergenic	lnc-TRIM43-7	372	15	URS00021A8627_29158	4.0e+03	56.1
	Contig_0178066	−450	Nucleus	Antisense	CASC15	15	–	–	–	–
	Contig_0090527_	−375	Cytoplasm	lincRNA/intergenic	lnc-PDLIM1-2	227	7	URS00021DB9AF_29158	3.7e+04	64.9
	Contig_0187540	−338	Nucleus	Intronic/sense	lnc-EIF4E3-7	89	–	–	–	–
	Contig_0058892_	−307	Nucleus	lincRNA/intergenic	LINC02372	826	27	URS00021CA876_29158	5.0e+03	65.0
	Contig_0145887	−204	Nucleus	lincRNA/intergenic	LINC01387	67	–	–	–	–
	Contig_0173437	−198	Nucleus	Antisense	Lnc-TNFRSF17-2	80	–	–	–	–
	Contig_0167250	−196	Nucleus	lincRNA/intergenic	lncRNA 1270	57	1	URS00021D1E6F_29158	3.6e+04	76.7
	Contig_0004931_	−187	Nucleus	lincRNA/intergenic	lnc-LRCH1-5	294	17	URS00021D7F17_29158	1.7e+03	60.9
	Contig_0184179	−180	Nucleus	Antisense	ATXN8OS	44	–	–	–	–

Table 3

Annotations for the top ten location-specific, differentially expressed lncRNAs identified through online database analysis. Labels: FC_{value} (Fold change value), MG (*Mytilus galloprovincialis*), LCo (local individuals form Cochamó), LYa (locals from Yaldad).

| Samples	Query lncRNA Contig	FC_{value}	lncLoc Location	LNCPedia Sequence Ontology class	LNCPedia & LncBook Gene Name	RNACentral Hits	RNACentral MG Hits	RNACentral MG ID	e-value	Identity (%)
LCo	Contig_0001041_	2191	Cytoplasm	lincRNA/intergenic	lnc-ARF1-3	754	2	URS00021BD1DA_29158	2.7e+03	63.0
	Contig_0157363	1262	Nucleus	lincRNA/intergenic	HSALNG0011272	97	–	–	–	–
	Contig_0077759_	1170	Nucleus	lincRNA/intergenic	lnc-NYAP2-9	868	3	URS0002196DB8_29158	3.5e+04	61.6
	Contig_0131765	1011	Nucleus	lincRNA/intergenic	lnc-PPP1R3D-1	212	64	URS00021BE1C5_29158	1.0e+01	59.7
	Contig_0067287_	937	Cytoplasm	lincRNA/intergenic	lnc-STYX-5	623	1	URS00021B73B1_29158	1.2e+05	59.5
	Contig_0040600_	788	Cytoplasm	Antisense	CIBAR1-DT	661	14	URS0002198EF4_29158	3.5e+04	60.0
	Contig_0142415	760	Nucleus	lincRNA/intergenic/ antisense	lnc-KDM6A-1	758	3	URS00021A7D7A_29158	5.0e+04	58.9
	Contig_0167970	641	Nucleus	Antisense	EGOT	132	–	–	–	–
	Contig_0104312_	621	Nucleus	lincRNA/intergenic	lnc-GJA5-1	841	3	URS00021B4BCF_29158	8.4e+04	58.6
	Contig_0076990_	612	Nucleus	lincRNA/intergenic	lnc-KHDRBS3-4	781	2	URS00021DD398_29158	2e+04	62.9
LYa	Contig_0126088_	−4338	Nucleus	lincRNA/intergenic	Lnc-NCAM2-13	544	3	URS00021A2660_29158	3.2e+0	71.1
	Contig_0154899	−3358	Nucleus	lincRNA/intergenic	HSALNT0181310	198	–	–	–	–
	Contig_0171681	−2488	Nucleus	lincRNA/intergenic	HSALNT0082546	599	4	URS00021D6B21_29158	2.3e+4	68.1
	Contig_0174947	−1977	Nucleus	lincRNA/intergenic	lnc-SOD2-2	130	–	–	–	–
	Contig_0110380_	−1695	Nucleus	lincRNA/intergenic	lnc-EPHA4-2	627	1	URS00021D8142_29158	5.1e+4	58.7
	Contig_0046952_	−1508	Nucleus	lincRNA/intergenic/ antisense	lnc-MYO1E-1	885	17	URS00021CB95B_29158	2.6e+0	90.4
	Contig_0095494_	−1506	Nucleus	lincRNA/intergenic/ antisense	HSALNT0054759	845	–	–	–	–
	Contig_0166992_	−1112	Nucleus	Intronic/sense	lnc-ITGA1-1	818	3	URS00021B2700_29158	1.9e+4	51.5
	Contig_0135620	−1046	Nucleus	lincRNA/intergenic	HSALNT0183595	782	18	URS00021E811F_29158	7.5e+1	50.3
	Contig_0125135_	−1028	Cytoplasm	Antisense	lnc-PAICS-3	656	4	URS00021EC6F0_29158	1.3e+5	65.6

identity with homologous sequences of *M. galloprovincialis* did not exceed 77 %. Still, one exception is the 98.2 % identity (e_{value} = 1e-124) of the intergenic antisense DE-lincRNA Contig_0118039_ (FC_{value} = 2480) in Cochamó gill samples, which overlaps the proximal *cis*-regulatory region of it neighbor gene (**Supplement 3**). Likewise, Table 3 shows the top ten DE-lncRNAs selected by FC_{value} for comparison by location. This table shows DE-lncRNAs sequences are probably nuclear and intergenic, with six antisenses. Also, 75 % of these sequences showed homology with *M. galloprovincialis* sequences, with an average e_{value} of 4e+04, and an average identity of 63 %.

3.6. Mapping DE-lncRNAs on chromosomes

Mapping DE-lncRNA sequences detected in Cochamó and Yaldad tissue samples against the chromosome-level genome sequence of *Mytilus chilensis* evidenced their distribution in almost all chromosomes (Fig. 3), except chromosome 7 (LCo_m) and 11 (LCo_g) of Cochamó samples (Fig. 3a). Similarly, DE-lncRNAs did not map in chromosomes 4 and 10 (LYa_m), chromosomes 9 and 12 (LYa_g), and chromosomes 5, 13, and 14 of both Yaldad tissues (Fig. 3b). Conversely, each location showed specific DE-lncRNAs differentially mapped in chromosomes 2, 6, and 11 for Cochamó and 3, 5, 8, 9, and 10 for Yaldad (Fig. 3c). Chromosomes 1, 4, and 13 showed no DE-lncRNAs.

3.7. Identification of DE-lncRNA neighboring protein-coding genes (NPC-genes)

The position of the DE-lncRNAs sequences within the chromosome-level *Mytilus chilensis* whole genome sequence allowed identify NPC-genes at a distance of 10 Kb up and downstream. Specifically, 16 genes neighboring DE-lncRNAs were detected in LCo_g samples and 17 in LCo_m. Likewise, four genes physically related to DE-lncRNAs were extracted and annotated from LYa_g samples and eight from LYa_m. Similarly, 11 NPC-genes were identified in Cochamó samples (LCo) and five in Yaldad (LYa). Table 4 lists by tissue the DE-lncRNAs and their FC_{value}, and their annotated NPC-genes using Swissprot/BLAST/Pfam and eggNOG databases. The latter describes their putative biological functions. From the list of DE-lncRNAs detected in LCo_g, the first two (Contig_0118039 and Contig_0099084) exhibit high FC_{value} (2481 and 1705 respectively) and have homologous sequences with genes encoding for the *Transient receptor potential cation channel* (BLAST OWF47104.1) and *Retrotransposon gag* (Pfam PF03732.16), proteins involved with ion channel transport (the former) and hydrolase activity on ester bonds (the latter). In LCo_m samples, the DE-lncRNAs Contig_0158861 (FCvalue = −516) and Contig_0183541 (FCvalue = −177) were distinguished. Interestingly, the latter is neighbored by four tandemly located copies annotated for the same gene coding for *Zinc finger MYM type 2* (BLAST XP_019637242.1). On the other hand, in LYa_g samples, the DE-lncRNAs Contig_0013111_ (FC_{value} = 306) and Contig_0145248 (FC_{value} = 206) were distinguished. The NPC-gene annotated for the former was an uncharacterized protein (SwissProt A0A0L8GUL6_OCTBM) related to chromosome segregation during meiosis (Pfam PF13889.5) and for the latter for *NAD-dependent epimerase/dehydratase* (Pfam PF01370.20). Similarly, for LYa_m samples, the DE-lncRNAs Contig_0090527_ (FC_{value} = −375) and Contig_0145887 (FC_{value} = −204) flank *Aspartyl protease* (Pfam PF13650.5) and *Alpha-8-like integrin* (BLAST XP_022307364.1), respectively. The first involves aspartate metabolism, and the second cell-to-cell interactions in the extracellular matrix.
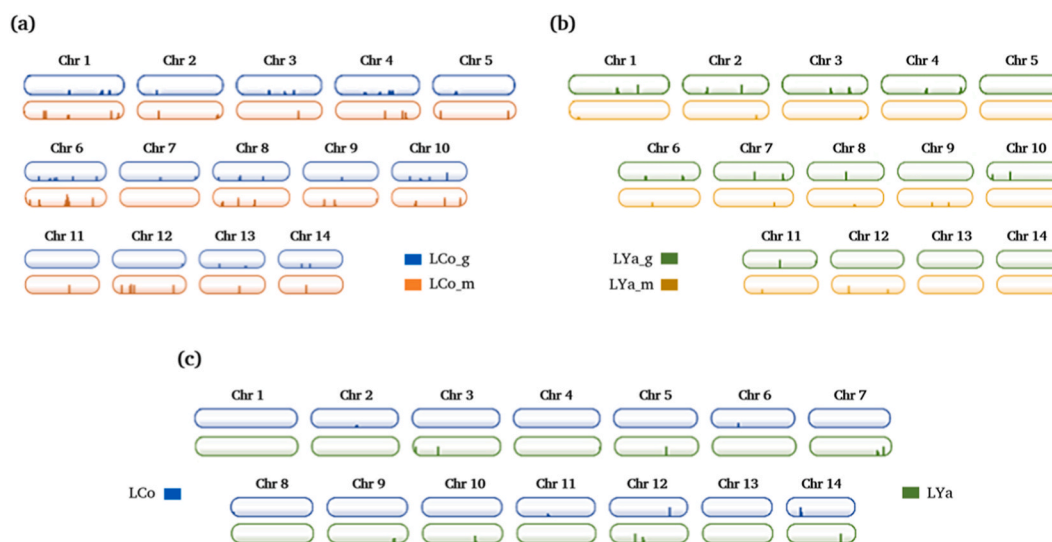
Fig. 3. Mapping significant DE lncRNAs on chromosomes of *Mytilus chilensis*.
Figure showing the mapping of the significant detected differential expressed lncRNAs (DE-lncRNAs) on chromosome sequences for both comparisons, by tissue (**a**) for Cochamó gill (LCo_g) and mantle (LCo_m) samples; likewise, for (**b**) Yaldad gills (LYa_g) and mantle (LYa_m) samples. Mapping location comparison is shown in (**c**). The little vertical lines on the chromosomes represent the DE-lncRNAs loci, with their height indicating the proximity between one lncRNA locus and another.

Table 4

Functional annotations derived from BLAST-NR, Pfam, and eggNOG databases for neighbor genes located within 10 kb upstream and downstream of differentially expressed lncRNAs, identified through tissue comparisons between Cochamó and Yaldad samples. Labels: FC$_{value}$ (Fold change value), NPC-gene (neighbor protein-coding gene), DE-lncRNA differentially expressed lncRNA), LCo_g/m (Cochamó gills/mantle), LYa_g/m (Yaldad gills/mantle).

Sample	DE-lncRNA	FC$_{value}$ DE-lncRNA	NPC-gene ID	Database	DataBase ID	Description	eggNOG_db ID	eggNOG_db description
LCo_g	Contig_0118039_	2481	MCH026002.1	BLAST NR	OWF47104.1	Transient receptor cation channel	32264.tetur04g05640.1	Ion channel involved with ion transport
	Contig_0118039_	2481	MCH026003.1	Pfam	PF03732.16	Retrotransposon gag protein	7668.SPU_005582-tr	hydrolase activity, acting on ester bonds
	Contig_0099084_	1705	MCH017627.1	BLAST NR	–	–	–	–
	Contig_0099084_	1705	MCH017628.1	BLAST NR	XP_022345076.1	ketohexokinase-like	1,026,970.XP_008833248.1	ketohexokinase activity
	Contig_0137093	249	MCH012672.1	BLAST NR	XP_022323514.1	uncharacterized protein	7739.XP_002607852.1	homophilic cell adhesion plasma membrane
	Contig_0137093	249	MCH012673.1	BLAST NR	XP_019928728.1	uncharacterized protein	7739.XP_002585627.1	carbohydrate binding
	Contig_0137093	249	MCH012674.1	BLAST NR	OWF56177.1	Protein crumbs-like 2	7739.XP_002607852.1	homophilic cell adhesion plasma membrane
	Contig_0121494_	226	MCH017100.1	BLAST NR	XP_022344764.1	fatty acid-binding protein	10160.XP_004643154.1	Belongs to the calycin superfamily
	Contig_0039019_	212	MCH026936.1	BLAST NR	XP_011428539.1	proteasome activator complex s3	132113.XP_003494521.1	Proteasome activator pa28 alpha subunit
	Contig_0109813_	201	MCH030029.1	BLAST NR	XP_021343247.1	serologically colon cancer antigen 3	6500.XP_005109887.1	endosome to plasma membrane transport
	Contig_0109813_	201	MCH030030.1	BLAST NR	XP_022335491.1	orexin receptor type 2-like	6500.XP_005110709.1	Transmembrane receptor (rhodopsin family)
	Contig_0077358_	161	MCH033585.1	BLAST NR	XP_021375028.1	galactoside fucosyltransferase 2-like	6412.HelroP113553	Belongs to the glycosyltransferase 11 family
	Contig_0012861_	138	MCH022479.1	Pfam	PF05225.15	helix-turn-helix, Psq domain	400682.PAC_15,715,526	DDE superfamily endonuclease
	Contig_0175647	112	MCH014345.1	Pfam	PF02037.26	SAP domain	7091.BGIBMGA007233-TA	Elongation complex protein 6
	Contig_0175647	112	MCH014346.1	BLAST NR	EKC31225.1	hypothetical protein CGI_10,007,117	7739.XP_002592569.1	Fibronectin type 3 domain
	Contig_0085502_	101	MCH025297.1	BLAST NR	XP_021364006.1	angiotensin-converting enzyme-like	7739.XP_002594682.1	negative regulation of gap junction assembly
LCo_m	Contig_0158861	−516	MCH001539.1	BLAST NR	EKC29556.1	hypothetical protein CGI_10,005,986	–	–
	Contig_0090188_	−509	MCH020558.1	BLAST NR	–	–	–	–
	Contig_0068815_	−348	MCH030760.1	Pfam	PF01841.18	Transglutaminase-like superfamily	6500.XP_005095535.1	coagulation factor XIII
	Contig_0139582	−344	MCH026804.1	Pfam	PF07701.13	Heme NO binding associated	10224.XP_002732877.1	Adenylyl-/guanylyl cyclase, catalytic domain
	Contig_0139582	−344	MCH026805.1	Pfam	PF13848.5	Thioredoxin-like domain	6500.XP_005099456.1	protein disulfide isomerase activity
	Contig_0053630_	−265	MCH031245.1	BLAST NR	–	–	–	–
	Contig_0183541	−177	MCH011024.1	BLAST NR	XP_019637242.1	zinc finger MYM-type protein 2-like	7739.XP_002595788.1	Domain of unknown function (DUF3504)
	Contig_0183541	−177	MCH011025.1	BLAST NR	XP_019637242.1	zinc finger MYM-type protein 2-like	7739.XP_002595788.1	Domain of unknown function (DUF3504)
	Contig_0183541	−177	MCH011026.1	BLAST NR	XP_019637242.1	zinc finger MYM-type protein 2-like	7739.XP_002595788.1	Domain of unknown function (DUF3504)
	Contig_0183541	−177	MCH011027.1	BLAST NR	XP_019637242.1	zinc finger MYM-type protein 2-like	7739.XP_002595788.1	Domain of unknown function (DUF3504)

Table 4 (*continued*)

Sample	DE-lncRNA	FC$_{value}$ DE-lncRNA	NPC-gene ID	Database	DataBase ID	Description	eggNOG_db ID	eggNOG_db description
	Contig_0127233_	−152	MCH000754.1	BLAST NR	OWF36549.1	Alpha-N-acetylglucosaminidase	6500.XP_005111892.1	alpha-N-acetylglucosaminidase activity
	Contig_0103326_	−134	MCH024459.1	BLAST NR	–	–	–	–
	Contig_0158168	−129	MCH008502.1	BLAST NR	XP_011433346.1	monocarboxylate transporter like	7955.ENSDARP00000124983	Solute carrier family (monocarboxylic acid)
	Contig_0112517_	−116	MCH024459.1	BLAST NR	–	–	–	–
	Contig_0165915	−108	MCH025707.1	BLAST NR	XP_021361462.1	uncharacterized protein	6412.HelroP192808	meiotic chromosome condensation
	Contig_0060146_	−106	MCH008363.1	BLAST NR	–	–	–	–
	Contig_0060146_	−106	MCH008364.1	Pfam	PF13857.5	Ankyrin repeats (many copies)	393283.XP_007835630.1	Heterokaryon incompatibility protein
LYa_g	Contig_0013111_	306	MCH029732.1	Pfam	PF13889.5	Chromosome segregation meiosis	7955.ENSDARP00000059207	Family sequence similarity 214, member A
	Contig_0145248	206	MCH006811.1	Pfam	PF01370.20	NAD epimerase/dehydratase	6500.XP_005095621.1	Short-chain dehydrogenases reductases
	Contig_0136663	149	MCH026671.1	BLAST NR	XP_013399112.1	isopentenyl-diphosphate isomerase	6500.XP_005089881.1	isopentenyl-diphosphate D-isomerase activity
	Contig_0136663	149	MCH029731.1	Pfam	PF00059.20	Lectin C-type domain	6500.XP_005097623.1	carbohydrate binding
LYa_m	Contig_0090527_	−375	MCH000032.1	Pfam	PF13650.5	Aspartyl protease	–	–
	Contig_0090527_	−375	MCH000033.1	BLAST NR	–	–	–	–
	Contig_0145887	−204	MCH025424.1	BLAST NR	XP_022307364.1	integrin alpha-8-like	6500.XP_005096876.1	integrin
	Contig_0173437	−198	MCH029387.1	BLAST NR	XP_022309849.1	uncharacterized protein	–	–
	Contig_0004931_	−187	MCH009563.1	Pfam	PF00025.20	ADP-ribosylation factor family	7668.SPU_017551-tr	C-terminal of Roc, COR, domain
	Contig_0165896	−160	MCH033992.1	Pfam	PF00811.17	Ependymin	7739.XP_002600936.1	Tetratricopeptide repeat
	Contig_0117722_	−151	MCH018786.1	BLAST NR	XP_021372766.1	interferon-induced GTPase 1-like	128390.XP_009465673.1	Interferon-induced very large GTPase 1-like
	Contig_0017998_	−103	MCH000360.1	BLAST NR	XP_019925357.1	uncharacterized protein	–	–

Table 5

Functional annotations of neighbor protein-coding genes (within 10 kb upstream and downstream) for location-specific differentially expressed lncRNAs between Cochamó and Yaldad samples, using BLAST-NR, Pfam, and eggNOG Databases. Labels: FCvalue (Fold change value), NPC-gene (neighbor protein-coding gene), DE-lncRNA (differentially expressed lncRNA), LCo (local individuals form Cochamó), LYa (locals from Yaldad).

Sample	DE-lncRNA	FC_{value} DE-lncRNA	NPC-gene ID	Database	DataBase ID	Description	eggNOG_db ID	eggNOG_db description
LCo	Contig_0001041_	2191	MCH012085.1	BLAST NR	OPL33288.3	hypothetical protein, partial	–	–
	Contig_0040600_	788	MCH009563.1	Pfam	PF00025.22	ADP-ribosylation factor family	7668.SPU_017551-tr	C-terminal of Roc, COR, domain
	Contig_0167970_	641	MCH015135.1	BLAST NR	–	–	–	–
	Contig_0167970_	641	MCH015136.1	BLAST NR	–	–	–	–
	Contig_0076990_	612	MCH012085.1	BLAST NR	OPL33288.1	hypothetical protein, partial	–	–
	Contig_0158965	300	MCH029901.1	Pfam	PF08241.11	Methyltransferase domain	345341.KUTG_08091	Methyltransferase domain
	Contig_0014623_	265	MCH009563.1	Pfam	PF00025.21	ADP-ribosylation factor family	7668.SPU_017551-tr	C-terminal of Roc, COR, domain
	Contig_0108805_	184	MCH012085.1	BLAST NR	OPL33288.2	hypothetical protein, partial	–	–
	Contig_0004931_	157	MCH009563.1	Pfam	PF00025.20	ADP-ribosylation factor family	7668.SPU_017551-tr	C-terminal of Roc, COR, domain
	Contig_0109074_	133	MCH025248.1	BLAST NR	–	–	–	–
	Contig_0105770_	109	MCH012085.1	BLAST NR	OPL33288.4	hypothetical protein, partial	–	–
LYa	Contig_0123915_	−323	MCH016823.1	BLAST NR	XP_011435502.1	peroxisomal membrane protein 2	6500.XP_005112377.1	Mpv17/PMP22 family
	Contig_0105992_	−150	MCH008552.1	BLAST NR	PFX22214.1	hypothetical SpisGene13271	–	–
	Contig_0105992_	−150	MCH008553.1	Pfam	PF00226.30	DnaJ domain	7897.ENSLACP00000001606	homolog subfamily B member
	Contig_0140828_	−120	MCH004830.1	BLAST NR	RUS77622.1	hypothetical protein, partial	6500.XP_005096629.1	DNA 5′-3′ RNA polymerase activity
	Contig_0092329_	−105	MCH029615.1	BLAST NR	XP_020907826.2	interferon-inducible GTPase	8153.XP_005952278.1	Interferon-inducible GTPase 5-like

Regarding the comparison between locations (Table 5), the DE-lncRNAs Contig_0001041_ ($FC_{value} = 2191$) and Contig_0158965 ($FC_{value} = 300$) of Cochamó samples are neighbors of the hypothetical protein AM593_02844 (BLAST OPL33288.3) and the *Methyltransferase domain* (Pfam PF08241.11), respectively. The latter is linked with the molecular methyl group transfer. In Yaldad samples, the DE-lncRNAs Contig_0140828 ($FC_{value} = -120.32$) neighbor the hypothetical protein EGW08_014622 (BLAST RUS77622.1), linked to DNA-directed 5 '-3' RNA polymerase activity (Pfam 6500.XP_005096629.1). Also, in Yaldad samples, the NPC-genes of the DE-lncRNAs Contig_0105992_ ($FC_{value} = -149.75$) and Contig_0092329_ ($FC_{value} = -104.79$) showed homology for *DnaJ domain coding gene* (Pfam PF00226.30), functionally linked with the stress-related Hsp70, and for *Interferon-inducible GTPase 5 isoform X2* (BLAST XP_020907826.2) related to the immune response.

3.8. GO analyses of DE-lncRNA neighboring protein-coding genes

In general, annotations using the KOBAS and REVIGO platforms yielded few homologous matches with KEGG and GO ID Terms for the sequences of the NPC-genes associated with DE-lncRNAs identified in location and tissue comparisons. For example, none of the neighboring DE-lncRNAs gene sequences found matches in the KEGG and GO databases for location comparison. The same occurred for the adjacent gene sequences of DE-lncRNAs detected in Yaldad gill samples. On the other hand, only two GO ID terms matched one (MCH017100.1) of the 16 NPC-genes of the DE-lncRNAs detected in Cochamó gill samples: GO:0007275 ($p_{value} = 0.012$), involved in multicellular organism development and GO:0016021 ($p_{value} = 0.093$), engaged with integrated components of the membrane. This neighbor gene MCH017100.1 (Table 4) of the significant DE-lncRNA Contig_0121494_ ($FC_{value} = 225.86$) was annotated for fatty acid-binding protein (BLAST XP_022344764.1) and recognized as belonging to the calycin superfamily (Pfam 10160. XP_004643154.1).

However, the sequences of the NPC-genes of the mantle DE-lncRNAs from both locations showed a higher number of matches of GO ID terms than in gills samples. The detected genes neighboring DE-lncRNAs of Cochamó mantle samples matched 58 GO ID terms, of which 31 related to biological processes, 16 to cellular components, and 11 to molecular functions. Neighboring gene sequences to DE-lncRNAs of Yaldad mantle samples matched 53 GO ID terms, 32 related to biological processes, 10 to cellular components, and 11 to molecular functions. The semantic distribution of the top ten most frequent GO ID terms of Fig. 4 shows resulting from the functional
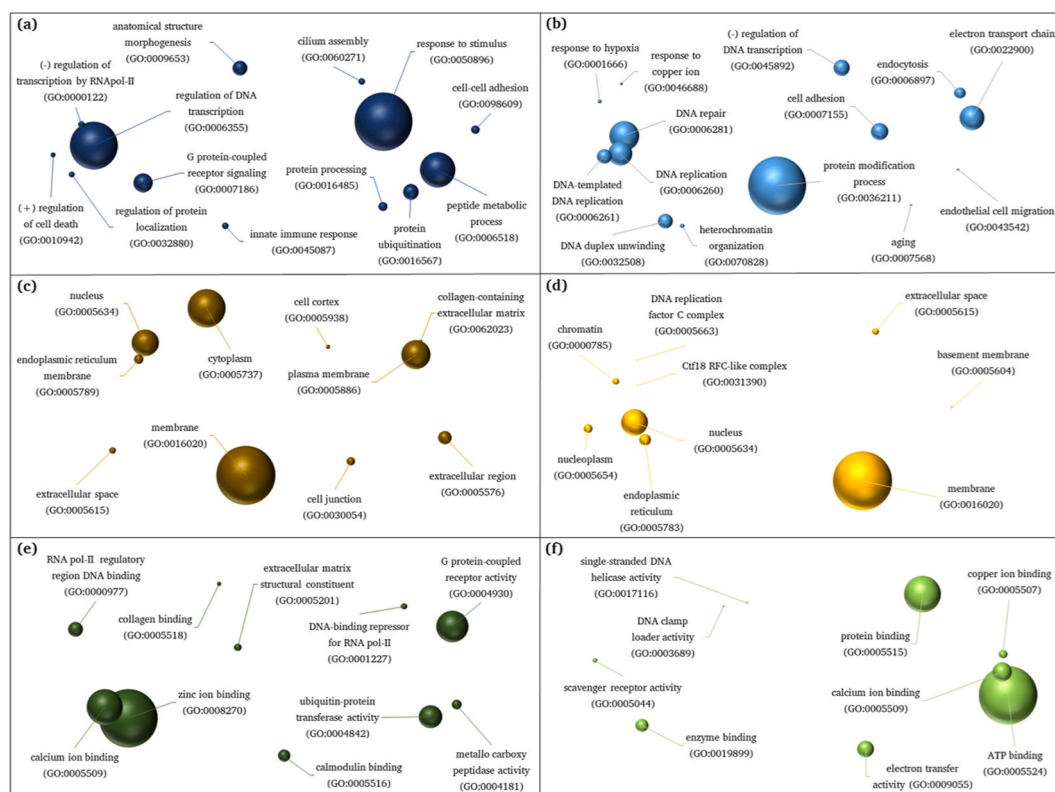
Fig. 4. GO annotations of lncRNA-neighboring genes.
Semantic visualization of GO ID term distribution, depicting functional annotations of differentially expressed neighboring protein-coding genes linked with differentially expressed lncRNAs within mantle samples from individuals in Cochamó (dark colors) and Yaldad (light colors). (**a**) and (**b**) indicate biological processes for samples from Cochamó and Yaldad, respectively, shown in blue. Cellular components are illustrated in brown for Cochamó (**c**) and Yaldad (**d**), while molecular functions are represented in green (**e**) for Cochamó and (**f**) for Yaldad. The size of each sphere represents the level of enrichment resulting from GO analysis. (For interpretation of the references to color in this figure legend, the reader is referred to the Web version of this article.)

annotations of protein-coding genes neighboring DE-lncRNAs identified in Cochamó (dark colors) and Yaldad mantle samples (light colors).

The biological processes most frequently represented by the NPC-genes in Cochamó mantle samples (Fig. 4a) were the response to stimulus (GO:0050896), regulation of DNA transcription (GO:0006355), peptide metabolic process (GO:0006518) and G protein-coupled receptor signaling (GO:0007186). In contrast, the genes most represented by NPC-genes in Yaldad mantle samples (Fig. 4b) are involved with the protein modification process (GO:0036211), DNA repair (GO:0006281), electron transport chain (GO:0022900) and DNA replication (GO:0006260). The cellular components most frequently represented by the NPC-genes in Cochamó mantle samples (Fig. 4c) involved the membrane (GO:0016020), cytoplasm (GO:0005737), plasma membrane (GO:0005886) and the nucleus (GO:0005634). The most represented in Yaldad mantle samples (Fig. 4d) related to the membrane (GO:0016020), nucleus (GO:0005634), endoplasmic reticulum (GO:0005783), and nucleoplasm (GO:0005654). Likewise, those molecular functions most represented in Cochamó mantle samples (Fig. 4e) involved the binding of the ions zinc (GO:0008270) and calcium (GO:0005509), G protein-coupled receptor activity (GO:0004930) and ubiquitin-protein transferase (GO:0004842). In contrast, the most represented GO ID terms in Yaldad mantle samples (Fig. 4f) related to the binding of ATP (GO:0005524), protein (GO:0005515), and calcium ion (GO:0005509), and electron transfer activity (GO:0009055) as well.

3.9. DE-lncRNA and NPC-genes expression comparison

The differentially expressed transcripts (DETs) between gill and mantle samples from both locations were mapped against the identified DE-lncRNAs neighboring gene sequences. Thus, 11 DETs were mapped in the 16 NPC-genes detected in Cochamó gill samples, and 12 were mapped in the 17 NPC-genes of the mantle. Similarly, one DET was mapped in the four NPC-genes detected in Yaldad gill samples, while nine DETs were mapped in the eight NPC-genes of the mantle. Table 6 contains comparative information on DE-lncRNAs whose NPC-genes present DETs. The coincidence between "+" and "-" signs indicates co-up-regulation. For example, the DE-lncRNA Contig_0137093 from Cochamó gill samples showed $FC_{value} = 249$, and its neighboring gene MCH012673.1 (Table 6a), annotated for a protein (BLAST XP_019928728.1) related to the carbohydrate-binding (eggNOG 7739.XP_002585627.1). This neighboring gene showed homology with DET _contig_384350 (1.555), whose $FC_{value} = 269$. The FC_{value} of DE-lncRNAs and NPC-genes for location comparison are listed in Table 6b. It should be noted that the estimated TPM values by RNA Seq analysis (as a proxy for gene expression patterns) have been validated through relative expression value analyses through comparison with their respective estimates by qRT-PCR (Supplement 4).

Table 6
Comparison of fold change values between differentially expressed lncRNAs and the homologous differentially expressed transcripts mapped to neighbor protein-coding genes. Labels: DE-lncRNA (differentially expressed lncRNA), FCvalue (Fold change value), NPC-gene (neighbor protein-coding gene), DET (differentially expressed transcript), LCo_g/m (Cochamó gills/mantle), LYa_g/m (Yaldad gills/mantle), LCo (local individuals form Cochamó), LYa (locals from Yaldad).

(a)					
Samples	DE-lncRNA	FC_{value} of DE-lncRNA	NPC-gene ID	DET ID	FC_{value} of DET
LCo_g	Contig_0137093	249	MCH012673.1	_contig_384350 (1.555)	270
	Contig_0039019_	212	MCH026936.1	_contig_128375 (55.1130)	256
	Contig_0077358_	161	MCH033585.1	_contig_189933 (733.1906)	377
	Contig_0085502_	101	MCH025297.1	_contig_8395 (66.3513)	−297
LCo_m	Contig_0090188_	−509	MCH020558.1	_contig_298946 (1.1632)	−121
	Contig_0068815_	−348	MCH030760.1	_contig_10076 (348.1669)	−879
	Contig_0139582	−344	MCH026805.1	_contig_13643 (1.1417)	−434
	Contig_0053630_	−265	MCH031245.1	_contig_33813 (526.849)	−304
	Contig_0183541	−177	MCH011025.1	_contig_7654 (1.2174)	−202
	Contig_0103326_	−134	MCH024459.1	_contig_11198 (1.2893)	−141
	Contig_0158168	−129	MCH008502.1	_contig_8395 (66.3513)	−297
	Contig_0060146_	−106	MCH008363.1	_contig_83322 (1.1137)	−126
LYa_g	Contig_0136663	149	MCH026671.1	_contig_205884 (1.619)	117
LYa_m	Contig_0090527_	−375	MCH000032.1	_contig_239 (1.352)	−452
	Contig_0004931_	−187	MCH009563.1	_contig_6721 (13.3328)	−282
	Contig_0165896	−160	MCH033992.1	_contig_67569 (1.901)	−103
(b)					
LCo	Contig_0040600_	788	MCH009563.1	_contig_15691 (3.1216)	241
	Contig_0167970	641	MCH015136.1	_contig_297269 (1.947)	483
	Contig_0158965	300	MCH029901.1	_contig_349632 (1.777)	363
	Contig_0014623_	265	MCH009563.1	_contig_21146 (1.849)	596
	Contig_0108805_	184	MCH012085.1	_contig_13374 (1.1317)	415
	Contig_0004931_	157	MCH009563.1	_contig_31549 (1.252)	461
	Contig_0109074_	133	MCH025248.1	_contig_44688 (36.1422)	24
LYa	Contig_0105992_	−150	MCH008553.1	_contig_301597 (109.904)	−17
	Contig_0092329_	−105	MCH029615.1	_contig_344086 (1.2375)	−164

4. Discussion

This research reports for the first time the differential expression of lncRNAs (DE-lncRNAs) in the genome of *Mytilus chilensis*, and their chromosomal distribution. Since the species supports a world-class aquaculture industry in southern Chile, identifying these epigenetic factors has relevance as they likely regulate gene expression in different biological, physiological, and ecological contexts. Although lncRNAs do not encode proteins, they engage with diverse cellular, molecular, and metabolic and, thus, can influence candidate genes controlling various ecologically relevant traits. The 43,011 sequences identified as lncRNAs represented about 22.7 % of the reference transcriptome (189,743 contigs) previously described [39], 19.91 % of which showed differential expression in the gill and mantle transcriptomes of Cochamó and Yaldad individuals, the seedbeds compared in this study. This percentage (19.91 %) is comparable to the 21.7 % observed in *M. galloprovincialis* individuals experimentally exposed to PAMPs antigenic molecules [27]. On average, 2.76 % of contigs of the transcriptomes analyzed in the species showed differential expression as DE lncRNAs, which is close to half the average value of the mitochondrial transcriptomes (4.5 %) of these same individuals [40].

Most DE lncRNAs detected in the transcriptomes of Cochamó and Yaldad individuals were classified as intervening and intergenic (lincRNAs), showing a widespread chromosome distribution. This distribution occurs within a genome marked by its size of 1.93 Gb, 34,530 protein-coding genes scattered across 14 chromosomes, and an abundant 56.7 % repetitive DNA content [66]. [73] conducted a phylogenetic analysis on lncRNA sequences from an echinoid sea urchin and 16 vertebrate species, classifying multiple lincRNAs as akin to transposable elements. These authors suggest that lincRNAs might be transcribed into stable mRNAs by linkage with regulatory genetic elements, possessing attributes encompassing transcription factor recruitment, splicing, cleavage, and polyadenylation. Given a substantial 56.7 % of repetitive DNA comprised in the *M. chilensis*, with a predominance of long terminal repeats (LTR) retrotransposons-like sequences, the broad-ranging chromosomal distribution of these DE-lincRNAs could be rationalized through transposable mechanisms, hypothesized to be associated with potential transposons and retrotransposon elements. For instance, the transposable Steamer-like elements linked to horizontally transmissible cancer found within the genome of this species [66] might play a role in elucidating the ubiquity of chromosome distribution observed in these DE-lincRNAs.

Since lncRNAs are described as having a rapid evolution rate, their sequences are generally not conserved, even in closely related species [73,74]. Accordingly, in most cases, the percentage of identity with homologous sequences of the sister species *M. galloprovincialis* did not exceed 77 %. However, the 98.2 % identity ($e_{value} = 1E-124$) of the intergenic DE lincRNA Contig_0118039 ($FC_{value} = 2480$) from Cochamó gills suggests that some lncRNA sequences may remain conserved due to an important role. Indeed, the DE-lincRNA Contig_0118039 fulfills a cytoplasmic functional role, overlapping the proximal *cis*-regulatory region of its neighboring gene annotated for *Transient receptor potential protein cation channel* (BLAST OWF47104.1), involved with the ion transport and ion channel activity (**Supplement 5**). Since this DE-lincRNA Contig_0118039 and its neighboring gene share the promoter region of their sequences, changes in the nucleotide sequence of this shared promoter region could affect the transcription of the encoding gene and the neighbor lncRNA.

Like DE-lincRNA Contig_0118039, most DE lncRNAs detected in the transcriptomes of Cochamó and Yaldad individuals are lincRNA/intergenic. Their mechanisms of action include promoter activation, activation and recruitment of transcription factor, or transcription interference, which regulate the RNA polymerase II function [9,10,14]. The regulation mechanism involved is known as *cis* gene regulation [12,16,17], as it affects the expression of its neighboring protein-coding genes (NPC-genes) [75]. This mechanism can explain the up-regulation of various lncRNAs and their linked NPC-genes detected in the transcriptomes of Cochamó and Yaldad individuals, such as those listed in Table 6. In this table, the "+" and "-" signs of FC_{values} of the DE-lncRNAs detected in each sample coincided with the FC_{values} of the NPC-genes, suggesting an up-regulatory effect of DE-lncRNAs seen in gill and mantle over their corresponding NPC-genes.

Without experimental evidence linking these lncRNAs functionally to their NPC-genes, it is challenging to associate the functional genomic differences between Cochamó and Yaldad individuals to the adaptive response to environmental variables. However, it may be suggested that lncRNAs and their NPC-genes may reflect a reaction to their contrasting ecological differences, as shown in Fig. 1. Such an assumption considers that multiple NPC-genes, modulated by their DE-lncRNAs, involve numerous biological processes, cellular components, and molecular functions that may influence fitness traits. Acknowledging the need to test fitness traits directly, e. g., knowing the role some gene products may play in ecologically relevant phenotypes, will undoubtedly enlighten the discussion. To provide a few examples, genes coding for *Ankyrin repeats* (many copies) influence heterokaryon incompatibility (Pfam PF13857.5); LOC110455591 affects the meiotic chromosome condensation (BLAST XP_021361462.1); *Interferon-induced very large GTPase 1-like* (BLAST XP_021372766.1) linked with host resistance, inflammation, diseases, and immune system. There are examples where one DE-lncRNA is flanked by more than one gene. The DE-lncRNA Contig_0183541 ($FC_{value} = -177$) presents four NPC-genes placed in tandem and are annotated for the same DNA-related transcription factor *Zinc finger MYM type 2* (BLAST XP_019637242.1). Such chromosome organization strongly suggests that their neighboring DE lncRNAs could influence the expression of these zinc finger MYM-type coding genes. However, the up-regulation of a given lncRNA could be related to its adjacent down-regulated gene, for example, the DE-lncRNA Contig_0085502 of Cochamó gill samples, as inferred for the unmatched "+" and "-" signs of their FC_{values}. This up-regulated lncRNA ($FC_{value} = 101$) showed their neighboring gene coding for *Angiotensin-converting enzyme-like*, as down-regulated ($FC_{value} = -297$). According to functional GO ID annotations, the down-regulation of this gene could cause a positive regulation of gap-junction assembly in these individuals. This observation is consistent with the Cochamó mantle GO annotations, in which biological processes such as cell-cell adhesion (GO:0098609), cellular components like cell junction (GO:0030054), and molecular functions of the extracellular matrix structural constituents (GO:0005201) were frequently over-represented.

Generally, gills from individuals sampled at both locations showed more mapped reads than their mantle tissue counterparts, suggesting that this tissue would have higher transcriptional activity. However, mantle samples from both locations were more

informative regarding the functional annotations of their NPC-genes, as evidenced by using multiple databases. It is plausible that employing less stringent filters in selecting DE-lncRNAs could yield a more comprehensive capture of information from the databases. Nevertheless, adopting more flexible filters carries the inherent risk of incorporating lncRNAs with lower fold change values that might hold relevant biological effects. Given their expression similarity to counterparts with lesser or null biological impact, the identification of these lncRNAs poses methodological challenges that could be addressed through alternative approaches (e.g., cloning) to assess this concern.

This study employed stringent filters to emphasize those lncRNAs exhibiting more pronounced and potentially striking differences within the biological context of individuals adapted to ecologically contrasting locations. Thus, DE-lncRNAs detected in the mantle likely influence the expression of several of their adjacent genes functionally linked to metabolism, intercellular communication, and genetic and environmental information processing. The biological processes, cellular components, and molecular functions putatively modulated by DE-lncRNAs (e.g., innate immune response, DNA repair and replication, cell junction, chromatin, G protein-coupled receptors, electron transport, and transfer chain) (Fig. 4) confirm observations previously reported for the whole transcriptome and mito-transcriptome of *M. chilensis* [39,40]. These studies also discussed the potential contribution of multiple differentially expressed genes to ecologically relevant traits. Additionally, the natural north-south oceanographic barriers of Chiloé Island (temperature, salinity, currents, chlorophyll-a concentration, and age of seawater) exert contrasting selective forces for the survival and reproductive performance of the mussel. Field and laboratory studies have evaluated the response of *M. chilensis* to temperature [64,76,77], salinity [38], acidification [61,62,78], and toxic substances [79]. Predators can also affect mussel survival [37,80–82].

In contrast to the assumption derived from the analysis of neutral population genetic markers (microsatellites), which suggests the presence of a single reproductive unit in southern Chile without distinct regional stocks, except for Punta Arenas in Magallanes [48], the findings of this study indicate that the biogeographic barriers between Cochamó and Yaldad maintain adaptive genomic differences among the local individuals of *M. chilensis*. These differences are not only evidenced in genic expressions and monomorphic genetic variants of their complete and mitochondrial transcriptomes [39,40], but also in the differential expression of epigenetic factors such as the DE-lncRNAs detected in this study. However, the most relevant aspect of this research is the low genetic divergence described for the different locations of this species [44–47] and the location-specific monomorphic genetic variants reported for the transcriptomes of Cochamó and Yaldad individuals provide an incomplete picture of their adaptive differences. Epigenetic factors like DE-lncRNAs offer a complementary view of these differences. Still, these heritable epigenetic factors can influence the expression of other genes, close or distant, without mediating modifications of the nucleotide sequences, which are a source for a faster response to climate change than genetic variation. Therefore, the identification and further analysis of the role of DE-lncRNAs in the Chilean blue mussel will provide insights into the sustainable management and exploitation of this relevant endemic species.

5. Conclusions

This study detected for the first time differentially expressed lncRNAs (DE-lncRNAs) from the transcriptomic analysis of gill and mantle of *Mytilus chilensis* individuals from two seedbeds affected by aquaculture (Cochamó and Yaldad). These lncRNAs represent another expression of the complex genomic architecture of *M. chilensis*. Despite representing 2.76 % of the whole transcriptome, these epigenetic factors play an active and regulatory role in gills and mantles in line with their critical functions. Given the fundamental role of gills (oxygen exchange, immune response) and mantles (shell biomineralization, locomotion) in the survival and reproduction of mussels, these DE-lncRNAs represent environment-influenced epigenetic factors related to habitat differences (e.g., temperature, salinity, currents, age of seawater). Such DE-lncRNAs could affect the expression of neighboring genes and provide evidence of the species's ability to cope with the multiple perturbations to which the species is exposed. Likewise, with the hundreds of monomorphic genetic variants detected in their transcriptomes, these lncRNAs provide an additional fast genomic response influencing tissue- and location-specific candidate adaptive NPC-gene expressions, metabolic and immune system functions, and genetic and environmental information processing. These epigenetic factors and their effect on the genomic functioning of *M. chilensis* could be helpful as population markers for the monitoring, conservation, and management of natural seedbeds, as well as to evaluate the impact on individuals' fitness when transplanted.

Data availability

Funding

CRediT authorship contribution statement

Marco Yévenes: Writing – review & editing, Writing – original draft, Visualization, Validation, Supervision, Software, Project administration, Methodology, Investigation, Formal analysis, Data curation, Conceptualization. **Cristian Gallardo-Escárate:**

Conceptualization, Writing – review & editing, Writing – original draft, Visualization, Validation, Software, Resources, Project administration, Investigation, Funding acquisition. **Gonzalo Gajardo:** Writing – review & editing, Writing – original draft, Supervision, Resources, Project administration, Investigation, Funding acquisition, Conceptualization.

Declaration of competing interest

The authors declare that they have no known competing financial interests or personal relationships that could have appeared to influence the work reported in this paper.

Acknowledgments

Appendix A. Supplementary data

Supplementary data to this article can be found online at https://doi.org/10.1016/j.heliyon.2023.e23695.

References

[1] H. Kokko, A. Chaturvedi, D. Croll, M.C. Fischer, F. Guillaume, S. Karrenberg, B. Kerr, G. Rolshausen, J. Stapley, Can evolution supply what ecology demands? Trends Ecol. Evol. 32 (2017) 187–197, https://doi.org/10.1016/j.tree.2016.12.005.
[2] O. Bossdorf, C.L. Richards, M. Pigliucci, Epigenetics for ecologists, Ecol. Lett. 11 (2007) 106–115, https://doi.org/10.1111/j.1461-0248.2007.01130.x.
[3] G.E. Hofmann, Ecological epigenetics in marine metazoans, Front. Mar. Sci. 4 (2017) 4, https://doi.org/10.3389/fmars.2017.00004.
[4] G.F. Lamka, A.M. Harder, M. Sundaram, T.S. Schwartz, M.R. Christie, J.A. DeWoody, J.R. Willoughby, Epigenetics in ecology, evolution, and conservation, Front. Ecol. Evol. 10 (2022), 871791, https://doi.org/10.3389/fevo.2022.871791.
[5] Y. Gao, Y. Chen, S. Li, X. Huang, J. Hu, D.G. Bock, A. Zhan, Complementary genomic and epigenomic adaptation to environmental heterogeneity, Mol. Ecol. 31 (2022) 3598–3612, https://doi.org/10.1111/mec.16500.
[6] P.B. Greenspoon, H.G. Spencer, L.K. M'Gonigle, Epigenetic induction may speed up or slow down speciation with gene flow, Evolution 76 (2022) 1170–1182, https://doi.org/10.1111/evo.14494.
[7] A. Necsulea, M. Soumillon, M. Warnefors, A. Liechti, T. Daish, U. Zeller, J.C. Baker, F. Grützner, H. Kaessmann, The evolution of lncRNA repertoires and expression patterns in tetrapods, Nature 505 (2014) 635–640, https://doi.org/10.1038/nature12943.
[8] C. Détrée, G. Núñez-Acuña, F. Tapia, C. Gallardo-Escárate, Long non-coding RNAs are associated with spatiotemporal gene expression profiles in the marine gastropod Tegula atra, Marine Genomics 33 (2017) 39–45, https://doi.org/10.1016/j.margen.2017.01.002.
[9] F. Kopp, J.T. Mendell, Functional classification and experimental dissection of long non-coding RNAs, Cell 172 (2018) 393–407, https://doi.org/10.1016/j.cell.2018.01.011.
[10] C.P. Ponting, P.L. Oliver, W. Reik, Evolution and functions of long non-coding RNAs, Cell 136 (2009) 629–641, https://doi.org/10.1016/j.cell.2009.02.006.
[11] N. Romero-Barrios, M.F. Legascue, M. Benhamed, F. Ariel, M. Crespi, Splicing regulation by long non-coding RNAs, Nucleic Acids Res. 46 (2018) 2169–2184, https://doi.org/10.1093/nar/gky095.
[12] H. Wu, L. Yang, L.-L. Chen, The diversity of long non-coding RNAs and their generation, Trends Genet. 33 (2017) 540–552, https://doi.org/10.1016/j.tig.2017.05.004.
[13] C.E. Ang, A.E. Trevino, H.Y. Chang, Diverse lncRNA mechanisms in brain development and disease, Curr Op Gen & Dev 65 (2020) 42–46, https://doi.org/10.1016/j.gde.2020.05.006.
[14] J.J. Quinn, H.Y. Chang, Unique features of long non-coding RNA biogenesis and function, Nat. Rev. Genet. 17 (2016) 47–62, https://doi.org/10.1038/nrg.2015.10.
[15] K.W. Vance, C.P. Ponting, Transcriptional regulatory functions of nuclear long non-coding RNAs, Trends Genetics 30 (2014) 348–355, https://doi.org/10.1016/j.tig.2014.06.001.
[16] I. Ulitsky, D.P. Bartel, lincRNAs: genomics, evolution, and mechanisms, Cell 154 (2013) 26–46, https://doi.org/10.1016/j.cell.2013.06.020.
[17] R.-W. Yao, Y. Wang, L.-L. Chen, Cellular functions of long non-coding RNAs, Nat. Cell Biol. 21 (2019) 542–551, https://doi.org/10.1038/s41556-019-0311-8.
[18] J. Huang, X. Luo, L. Zeng, Z. Huang, M. Huang, W. You, C. Ke, Expression profiling of lncRNAs and mRNAs reveals regulation of muscle growth in the Pacific abalone, Haliotis discus hannai, Sci. Rep. 8 (2018), 16839, https://doi.org/10.1038/s41598-018-35202-z.
[19] Z. Hongkuan, T. Karsoon, L. Shengkang, L. Hongyu, Z. Huaiping, The functional roles non- molluscs, Gene 768 (2021), 145300, https://doi.org/10.1016/j.gene.2020.145300.
[20] S. Valanne, T.S. Salminen, M. Järvelä-Stölting, L. Vesala, M. Rämet, Immune-inducible non-coding RNA molecule lincRNA-IBIN connects immunity and metabolism in D. melanogaster, PLoS 15 (2019), e1007504, https://doi.org/10.1371/journal.ppat.1007504.
[21] P. Zhang, L. Cao, R. Zhou, X. Yang, M. Wu, The lncRNA Neat1 promotes activation of inflammasomes macrophages, Nat. Commun. 10 (2019) 1495, https://doi.org/10.1038/s41467-019-09482-6.
[22] P. Pereiro, R. Lama, R. Moreira, V. Valenzuela-Muñoz, C. Gallardo-Escárate, B. Novoa, A. Figueras, Potential involvement of lncRNAs in the modulation of the transcriptome response to nodavirus challenge in European sea bass (Dicentrarchus labrax L.), Biology 9 (2020) 165, https://doi.org/10.3390/biology9070165.
[23] E. Tarifeño-Saldivia, D. Valenzuela-Miranda, C. Gallardo-Escárate, In the shadow: the emerging role of long non-coding RNAs in the immune response of Atlantic salmon, Devel & Comparat Immun 73 (2017) 193–205, https://doi.org/10.1016/j.dci.2017.03.024.
[24] V. Valenzuela-Muñoz, P. Pereiro, M. Álvarez-Rodríguez, C. Gallardo-Escárate, A. Figueras, B. Novoa, Comparative modulation of lncRNAs in wild-type and rag1-heterozygous mutant zebrafish exposed to immune challenge with spring viraemia of carp virus (SVCV), Sci. Rep. 9 (2019), 14174, https://doi.org/10.1038/s41598-019-50766-0.
[25] X.-D. Huang, J. Dai, K. Lin, M. Liu, H. Ruan, H. Zhang, W. Liu, M.-X. He, M. Zhao, Regulation of IL-17 by lncRNA of IRF-2 in the pearl oyster, Fish Shellfish Immunol. 81 (2018) 108–112, https://doi.org/10.1016/j.fsi.2018.07.020.
[26] W. Sun, J. Feng, Differential lncRNA expression profiles reveal the potential roles of lncRNAs in antiviral immune response of Crassostrea gigas, Fish Shellfish Immunol. 81 (2018) 233–241, https://doi.org/10.1016/j.fsi.2018.07.032.

[27] P. Pereiro, R. Moreira, B. Novoa, A. Figueras, Differential expression of long non-coding RNA (lncRNA) in mediterranean mussel (Mytilus galloprovincialis) hemocytes under immune stimuli, Genes 12 (2021) 1393, https://doi.org/10.3390/genes12091393.

[28] H. Zhang, G. Yao, M. He, LncRNA7467 participated in shell biomineralization in pearl oyster, Aquaculture Reports 27 (2022), 101398, https://doi.org/10.1016/j.aqrep.2022.101398.

[29] D. Feng, Q. Li, H. Yu, L. Kong, S. Du, Transcriptional profiling of long non-coding RNAs in mantle of Crassostrea gigas and their association with shell pigmentation, Sci. Rep. 8 (2018) 1436, https://doi.org/10.1038/s41598-018-19950-6.

[30] H. Yu, X. Zhao, Q. Li, Genome-wide identification and characterization of long intergenic non-coding RNAs and their potential association with larval development in the Pacific oyster, Sci. Rep. 6 (2016), 20796, https://doi.org/10.1038/srep20796.

[31] A. Saco, M. Rey-Campos, B. Novoa, A. Figueras, Transcriptomic response of mussel gills after a Vibrio splendidus infection demonstrates their role in the immune response, Front. Immunol. 11 (2020), 615580, https://doi.org/10.3389/fimmu.2020.615580.

[32] B. Hargrave, L. Doucette, P. Cranford, B. Law, T. Milligan, Influence of mussel aquaculture on sediment organic enrichment in a nutrient-rich coastal embayment, Mar. Ecol. Prog. Ser. 365 (2008) 137–149, https://doi.org/10.3354/meps07636.

[33] C. Vinagre, V. Mendonça, L. Narciso, C. Madeira, Food web of the intertidal rocky shore of the west Portuguese coast – determined by stable isotope analysis, Marine Envir Research 110 (2015) 53–60, https://doi.org/10.1016/j.marenvres.2015.07.016.

[34] J.D. Gaitán-Espitia, J.F. Quintero-Galvis, A. Mesas, G. D'Elía, Mitogenomics of southern hemisphere blue mussels (Bivalvia: pteriomorphia): insights into the evolutionary characteristic M. edulis complex, Sci. Rep. 6 (2016), 26853, https://doi.org/10.1038/srep26853.

[35] M.A. Larraín, M. Zbawicka, C. Araneda, J.P.A. Gardner, R. Wenne, Native and invasive taxa on the Pacific coast of South America: impacts on aquaculture, traceability and biodiversity blue mussels, Evol Appl 11 (2018) 298–311, https://doi.org/10.1111/eva.12553.

[36] C.A. Molinet, M.A.D. Gomez, C.B.A. Muñoz, L.E.C. Pérez, S.L.M. Arribas, M.P.A. Opazo, E.J.E.N. Huaquin, Spatial distribution pattern of Mytilus chilensis beds in the Reloncaví fjord: hypothesis on associated processes, Rev. Chil. Hist. Nat. 88 (2015) 11, https://doi.org/10.1186/s40693-015-0041-7.

[37] J. Curelovich, G.A. Lovrich, J.A. Calcagno, The role of the predator Trophon geversianus in an intertidal population of Mytilus chilensis in a rocky shore of the Beagle Channel, Tierra del Fuego, Argentina, Mar. Biol. Res. 12 (2016) 1053–1063, https://doi.org/10.1080/17451000.2016.1228976.

[38] C. Duarte, J.M. Navarro, P.A. Quijón, D. Loncon, R. Torres, P.H. Manríquez, M.A. Lardies, C.A. Vargas, N.A. Lagos, The energetic physiology of juvenile mussels, Mytilus chilensis (Hupe): the prevalent role of salinity under current and predicted pCO2 scenarios, Env Pollution 242 (2018) 156–163, https://doi.org/10.1016/j.envpol.2018.06.053.

[39] M. Yévenes, G. Núñez-Acuña, C. Gallardo-Escárate, G. Gajardo, Adaptive differences in gene expression in farm-impacted seedbeds of the native blue mussel Mytilus chilensis, Front. Genet. 12 (2021), 666539, https://doi.org/10.3389/fgene.2021.666539.

[40] M. Yévenes, G. Núñez-Acuña, C. Gallardo-Escárate, G. Gajardo, Adaptive mitochondrial genome functioning in ecologically different farm-impacted natural seedbeds of the endemic blue mussel Mytilus chilensis, Comp. Biochem. Physiol. Genom. Proteomics 42 (2022), 100955, https://doi.org/10.1016/j.cbd.2021.100955.

[41] M. Ruiz, E. Tarifeño, A. Llanos-Rivera, C. Padget, B. Campos, Efecto de la temperatura en el desarrollo embrionario y larval del mejillón, Mytilus galloprovincialis, Rev. Biol. Mar. Oceanogr. 43 (1) (2008) 51–61, https://doi.org/10.4067/S0718-19572008000100006.

[42] J.E. Toro, A.C. Alcapan, A.M. Vergara, J.A. Ojeda, Heritability estimates of larval and spat shell height in the Chilean blue mussel (Mytilus chilensis Hupe 1854) produced under laboratory conditions, Aquac Res 35 (2004) 56–61, https://doi.org/10.1111/j.1365-2109.2004.00985.x.

[43] A. Barría, P. Gebauer, C. Molinet, Variabilidad espacial y temporal del suministro larval de mitílidos en el Seno de Reloncaví, Rev. Biol. Mar. Oceanogr. 47 (2012) 461–473, https://doi.org/10.4067/S0718-19572012000300009.

[44] C. Araneda, M.A. Larraín, B. Hecht, S. Narum, Adaptive genetic variation distinguishes Chilean blue mussels (Mytilus chilensis) from different marine environments, Ecol. Evol. 6 (2016) 3632–3644, https://doi.org/10.1002/ece3.2110.

[45] M.P. Astorga, J. Vargas, A. Valenzuela, C. Molinet, S.L. Marín, Population genetic structure and differential selection in mussel Mytilus chilensis, Aquac Res 49 (2018) 919–927, https://doi.org/10.1111/are.13538.

[46] M.P. Astorga, L. Cárdenas, M. Pérez, J.E. Toro, V. Martínez, A. Farías, I. Uriarte, Complex spatial genetic connectivity of mussels Mytilus chilensis along the southeastern pacific coast and its importance for resource management, J. Shellfish Res. 39 (2020) 77, https://doi.org/10.2983/035.039.0108.

[47] M.A. Larraín, N.F. Díaz, C. Lamas, C. Uribe, C. Araneda, Traceability of mussel (Mytilus chilensis) in southern Chile using microsatellite molecular markers and assignment algorithms, Exploratory survey, Food Research International 62 (2014) 104–110, https://doi.org/10.1016/j.foodres.2014.02.016.

[48] B. Díaz-Puente, A. Pita, J. Uribe, J. Cuéllar-Pinzón, R. Guiñez, P. Presa, A biogeography-based management for Mytilus chilensis: the genetic hodgepodge of Los Lagos versus the pristine hybrid zone of the Magellanic ecotone, Aquat. Conserv. Mar. Freshw. Ecosyst. 30 (2020) 412–425, https://doi.org/10.1002/aqc.3271.

[49] E. Gonzalez-Poblete, F.C.F. Hurtado, S.C. Rojo, C.R. Norambuena, Blue mussel aquaculture in Chile: small- or large-scale industry? Aquaculture 493 (2018) 113–122, https://doi.org/10.1016/j.aquaculture.2018.04.026.

[50] M.I. Castillo, U. Cifuentes, O. Pizarro, L. Djurfeldt, M. Caceres, Seasonal hydrography and surface outflow in a fjord with deep sill: the Reloncaví fjord, Chile (preprint). All Depths/In situ Observations/Shelf Seas/Temperature, Salinity and Density Fields (2015), https://doi.org/10.5194/osd-12-2535-2015.

[51] C. Lara, G.S. Saldías, F.J. Tapia, J.L. Iriarte, B.R. Broitman, Interannual variability in temporal patterns of Chlorophyll–a and their potential influence on the supply of mussel larvae to inner waters in northern Patagonia (41–44°S), J. Mar. Syst. 155 (2016) 11–18, https://doi.org/10.1016/j.jmarsys.2015.10.010.

[52] V. Martínez, C. Lara, N. Silva, V. Gudiño, V. Montecino, Variability of environmental heterogeneity in northern Patagonia, Chile: effects on the spatial distribution, size structure and abundance of chlorophyll-a, Rev. Biol. Mar. Oceanogr. 50 (2015) 39–52, https://doi.org/10.4067/S0718-19572015000100004.

[53] J. Ottenburghs, The genic view of hybridization in the Anthropocene, Evol Appl 14 (2021) 2342–2360, https://doi.org/10.1080/eva.13223.

[54] C.P. Aranda, M. Yévenes, C. Rodriguez-Benito, F.A. Godoy, M. Ruiz, V. Cachicas, Distribution and growth of Vibrio parahaemolyticus in southern Chilean clams (venus antiqua) and blue mussels (Mytilus chilensis), Foodborne Path and Disease 12 (2015) 1–7, https://doi.org/10.1089/fpd.2014.1819.

[55] A.P. Gray, I.A.N. Lucas, R. Seed, C.A. Richardson, Mytilus edulis chilensis infested with Coccomyxa parasitica (Chlorococcales, Coccomyxaceae), J. Molluscan Stud. 65 (1999) 289–294, https://doi.org/10.1093/mollus/65.3.289.

[56] J.M. Blanc, C. Molinet, R. Subiabre, P.A. Díaz, Cadmium determination in Chilean blue mussels Mytilus chilensis: implications for environmental and agronomic interest, Mar. Pollut. Bull. 129 (2018) 913–917, https://doi.org/10.1016/j.marpolbul.2017.10.048.

[57] C. Détrée, G. Núñez-Acuña, S. Roberts, C. Gallardo-Escárate, Uncovering the complex transcriptome response of Mytilus chilensis against saxitoxin: implications of harmful algal blooms on mussel populations, PLoS One 11 (2016), e0165231, https://doi.org/10.1371/journal.pone.0165231.

[58] C.D. Harvell, C.E. Mitchell, J.R. Ward, S. Altizer, A.P. Dobson, R.S. Ostfeld, M.D. Samuel, Climate warming and disease risks for terrestrial and marine biota, Science 296 (2002) 2158–2162, https://doi.org/10.1126/science.1063699.

[59] A.K. Hüning, F. Melzner, J. Thomsen, M.A. Gutowska, L. Krämer, S. Frickenhaus, P. Rosenstiel, H.-O. Pörtner, E.E.R. Philipp, M. Lucassen, Impacts of seawater acidification on mantle gene expression patterns of the Baltic Sea blue mussel, Mar Biol 160 (2013) 1845–1861, https://doi.org/10.1007/s00227-012-1930-9.

[60] M. Vihtakari, I. Hendriks, J. Holding, P. Renaud, C. Duarte, J. Havenhand, Effects of ocean acidification and warming on sperm activity and early life stages of the mediterranean mussel (Mytilus galloprovincialis), Water 5 (2013) 1890–1915, https://doi.org/10.3390/w5041890.

[61] N. Castillo, L.M. Saavedra, C.A. Vargas, C. Gallardo-Escárate, C. Détrée, Ocean acidification and pathogen exposure modulate the immune response of the edible mussel M. chilensis, Fish & Shellf Imm 70 (2017) 149–155, https://doi.org/10.1016/j.fsi.2017.08.047.

[62] R. Díaz, M.A. Lardies, F.J. Tapia, E. Tarifeño, C.A. Vargas, Transgenerational effects of pCO2-driven ocean acidification on adult mussels Mytilus chilensis modulate physiological response to multiple stressors in larvae, Front. Physiol. 9 (2018) 1349, https://doi.org/10.3389/fphys.2018.01349.

[63] M. Malachowicz, R. Wenne, Mantle transcriptome sequencing of Mytilus spp. and identificat biomineralization genes, PeerJ 6 (2019) e6245, https://doi.org/10.7717/peerj.6245.

[64] R. Mlouka, J. Cachot, S. Sforzini, C. Oliveri, K. Boukadida, C. Clerandeau, B. Pacchioni, C. Millino, A. Viarengo, M. Banni, Molecular mechanisms underlying the effects of temperature increase on Mytilus sp. and their hybrids at early larval stages, Sci of Total Env 708 (2020), 135200, https://doi.org/10.1016/j.scitotenv.2019.135200.

[65] N. Jahnsen-Guzmán, N.A. Lagos, M.A. Lardies, C.A. Vargas, C. Fernández, V.A. San Martín, L. Saavedra, L.A. Cuevas, P.A. Quijón, C. Duarte, Environmental refuges increase performance of juvenile mussels Mytilus chilensis: implications for mussel seedling and farming strategies, Sci. Total Environ. 751 (2021), 141723, https://doi.org/10.1016/j.scitotenv.2020.141723.

[66] C. Gallardo-Escárate, V. Valenzuela-Muñoz, G. Nuñez-Acuña, D. Valenzuela-Miranda, F. Tapia, M. Yévenes, G. Gajardo, J.E. Toro, P.A. Oyarzún, G. Arriagada, B. Novoa, A. Figueras, S. Roberts, M. Gerdol, Chromosome-level genome assembly of the blue mussel Mytilus chilensis reveals molecular signatures facing the marine environment, Genes 14 (2023) 876, https://doi.org/10.3390/genes14040876.

[67] E. Pinilla, M.I. Castillo, I. Pérez-Santos, O. Venegas, A. Valle-Levinson, Water age variability in a Patagonian fjord, J. Mar. Syst. 210 (2020), 103376, https://doi.org/10.1016/j.jmarsys.2020.103376.

[68] L. Wang, H.J. Park, S. Dasari, S. Wang, J.-P. Kocher, W. Li, CPAT: coding-Potential Assessment Tool using an alignment-free logistic regression model, Nucleic Acids Res. 41 (6) (2013) e74, https://doi.org/10.1093/nar/gkt006.

[69] E. Afgan, D. Baker, M. van den Beek, D. Blankenberg, D. Bouvier, M. Čech, J. Chilton, D. Clements, N. Coraor, C. Eberhard, B. Grüning, A. Guerler, J. Hillman-Jackson, G. Von Kuster, et al., The Galaxy platform for accessible, reproducible and collaborative biomedical analyses: 2016, Nucleic Acids Res. 44 (2016) W3–W10, https://doi.org/10.1093/nar/gkw343.

[70] Z. Cao, X. Pan, Y. Yang, Y. Huang, H.-B. Shen, The lncLocator: a subcellular localization predictor for long non-coding RNAs based on a stacked ensemble classifier, Bioinformatics 34 (2018) 2185–2194, https://doi.org/10.1093/bioinformatics/bty085.

[71] D. Bu, H. Luo, P. Huo, Z. Wang, S. Zhang, Z. He, Y. Wu, L. Zhao, J. Liu, J. Guo, S. Fang, W. Cao, L. Yi, Y. Zhao, L. Kong, KOBAS-i: intelligent prioritization and exploratory visualization of biological functions for gene enrichment analysis, Nucleic Acids Res. 49 (2021) W317–W325, https://doi.org/10.1093/nar/gkab447.

[72] F. Supek, M. Bošnjak, N. Škunca, T. Šmuc, REVIGO summarizes and visualizes long gene ontology, PLoS One 6 (2011), e21800, https://doi.org/10.1371/journal.pone.0021800.

[73] H. Hezroni, D. Koppstein, M.G. Schwartz, A. Avrutin, D.P. Bartel, I. Ulitsky, Principles of long non-coding RNA evolution derived from direct comparison of transcriptomes 17 species, Cell Rep. 11 (2015) 1110–1122, https://doi.org/10.1016/j.celrep.2015.04.023.

[74] R.B.-T. Perry, I. Ulitsky, The functions of long non-coding RNAs in development and stem cells, Development 143 (2016) 3882–3894, https://doi.org/10.1242/dev.140962.

[75] Z. Zheng, W. Li, J. Xu, B. Xie, M. Yang, H. Huang, H. Li, Q. Wang, LncMSEN1, a mantle-specific LncRNA participating in nacre formation and response to polyI:C stimulation in pearl oyster Pinctada fucata martensii, Fish Shellfish Immunol. 96 (2020) 330–335, https://doi.org/10.1016/j.fsi.2019.12.015.

[76] C. Duarte, J.M. Navarro, K. Acuña, R. Torres, P.H. Manríquez, M.A. Lardies, C.A. Vargas, N.A. Lagos, V. Aguilera, Combined effects of temperature and ocean acidification on the juvenile individuals of the mussel Mytilus chilensis, J. Sea Res. 85 (2014) 308–314, https://doi.org/10.1016/j.seares.2013.06.002.

[77] J.M. Navarro, C. Duarte, P.H. Manríquez, M.A. Lardies, R. Torres, K. Acuña, C.A. Vargas, N.A. Lagos, Ocean warming and elevated carbon dioxide: multiple stressor impacts on juvenile mussels from southern Chile, ICES (Int. Counc. Explor. Sea) J. Mar. Sci. 73 (2016) 764–771, https://doi.org/10.1093/icesjms/fsv249.

[78] C. Mellado, O.R. Chaparro, C. Duarte, P.A. Villanueva, A. Ortiz, N. Valdivia, R. Torres, J.M. Navarro, Ocean acidification exacerbates the effects of paralytic shellfish toxins on the fitness of the edible mussel Mytilus chilensis, Sci. Total Environ. 653 (2019) 455–464, https://doi.org/10.1016/j.scitotenv.2018.10.399.

[79] G. Núñez-Acuña, A.E. Aballay, H. Hégaret, A.P. Astuya, C. Gallardo-Escárate, Transcriptional responses of Mytilus chilensis exposed in vivo to saxitoxin (STX), J. Molluscan Stud. 79 (2013) 323–331, https://doi.org/10.1093/mollus/eyt030.

[80] L. Riccialdelli, S.D. Newsome, M.L. Fogel, D.A. Fernández, Trophic interactions and food web structure of a subantarctic marine food web in the Beagle Channel: bahía Lapataia, Argentina, Pol Biol 40 (2017) 807–821, https://doi.org/10.1007/s00300-016-2007-x.

[81] A.A. Robson, C. Garcia De Leaniz, R.P. Wilson, L.G. Halsey, Behavioural adaptations of mussels to varying levels of food availability and predation risk, J. Molluscan Stud. 76 (2010) 348–353, https://doi.org/10.1093/mollus/eyq025.

[82] N. Uzkiaga, P. Gebauer, E. Niklitschek, et al., Predation of the crab Acanthocyclus albatrossis on seeds of the bivalve Mytilus chilensis under different environmental conditions: importance of prey and predator size, J. Exp. Mar. Biol. Ecol. 551 (2022), 151730, https://doi.org/10.1016/j.jembe.2022.151730.

Abbreviation list

DE-lncRNA: Differentially expressed long non-coding RNA
FCvalue: Fold change value
FDR pvalue: False discovery rate pvalue
GO: Gene ontology
PAMPs: Pathogen-associated molecular patterns
mGV: Monomorphic genetic variants
NPC-genes: Neighboring protein-coding genes
DETs: Differentially expressed transcripts
TPM: Transcript per million